High paleointensities for the Canary Islands constrain the Levant geomagnetic high

Lennart V. de Groot[1]*, Annemarieke Béguin[1], Martha E. Kosters[1], Elenora M. van Rijsingen[1], Erzsébet L.M. Struijk[1], Andrew J. Biggin[2], Elliot A. Hurst[2], Cor G. Langereis[1], Mark J. Dekkers[1]

1. Paleomagnetic laboratory Fort Hoofddijk, Department of Earth Sciences, Utrecht University, Budapestlaan 17, 3584 CD Utrecht, the Netherlands

2. Geomagnetism Laboratory, School of Environmental Sciences, University of Liverpool, Oliver Lodge Labs, Oxford Street, Liverpool L69 7ZE, UK

* Corresponding author: l.v.degroot@uu.nl

Highlights

- The 'multi-method paleointensity approach' applied to lavas from the Canary Islands
- A reliable paleointensity obtained for 60% of all cooling units sampled
- The influence of the Levant intensity high extends 50-60° to the west
- A possible westward movement of the Levant intensity high
- An updated calibration formula for the pseudo-Thellier method for lavas

Abstract

Understanding the behavior of enigmatic geomagnetic traits such as the Levant intensity high is currently challenged by a lack of full vector records of regional variations in the geomagnetic field. Here we apply the recently proposed multi-method paleointensity approach to a suite of 19 lavas from the Canary Islands dating between ~4000 BC and 1909 AD. Our new record reveals high paleointensities (VADMs >120 ZAm^2) coinciding with and shortly after the peak in geomagnetic intensity in the Levant at ~1000 BC. Furthermore our data suggests a westward movement of this geomagnetic phenomenon at a rate of 6.7-12° per century. In addition to IZZI-Thellier, microwave-Thellier and the multi-specimen method, the calibrated pseudo-Thellier method is an important part of the multi-method paleointensity approach. The calibration of this relative paleointensity method was derived from a suite of Hawaiian lavas; it is improved with the results of the Canarian cooling units. Pseudo-Thellier results from samples with very low Curie temperature (<150 °C), however, cannot be reliably converted to absolute paleointensity estimates. The multi-method paleointensity approach yielded a reliable estimate for ~60% of the flows sampled – an unusually high success rate for a paleointensity study involving lavas.

1. Introduction

Obtaining reliable paleointensities from volcanic edifices is notoriously difficult, despite recent methodological developments (e.g. Hill and Shaw, 1999; Riisager and Riisager, 2001; Tauxe and Staudigel, 2004; Dekkers and Böhnel, 2006; Fabian and Leonhardt, 2010; de Groot et al., 2012; Paterson et al., 2014) Yet, such records are indispensible to improve the accuracy of models that describe the behavior of the geomagnetic field during the Holocene, since igneous rocks are the only absolute recorders of the intensity of the geomagnetic field available around the globe and throughout geologic history. Paleointensity results of many flows have to be discarded because they do not satisfy certain quality criteria (Selkin and Tauxe, 2000; Biggin et al., 2007; de Groot et al, 2014; Paterson et al., 2014), often due to thermochemical alteration induced by the laboratory heating of the samples required for paleointensity experiments. It was recently shown that combining different paleointensity methods, including a non-heating calibrated pseudo-Thellier approach, significantly increases the success rate in obtaining reliable paleointensity estimates from lavas (de Groot et al., 2013). This 'multi-method paleointensity approach' consists of the IZZI-Thellier protocol (Tauxe and Staudigel, 2004), microwave Thellier experiments (Hill and Shaw, 1999; 2000), the domain state corrected multispecimen method (MSP-DSC) (Dekkers and Böhnel, 2006; Fabian and Leonhardt, 2010) and the calibrated pseudo-Thellier technique (de Groot et al., 2013).

The Canarian archipelago (28.1 ° N, 15.4 ° W) constitutes a suite of well-dated Holocene volcanic cooling units, but relatively little work has been done in terms of paleointensity on Holocene flows. Recently, Kissel et al. (2015) presented an extensive data set of paleodirections obtained from lavas sampled at Tenerife and Gran Canaria. Here we apply the multi-method paleointensity approach (de Groot et al., 2013) to 19 Holocene lavas from the islands of Tenerife and Gran Canaria (Canary Islands, Spain) to derive their full paleomagnetic vector. We focus particularly on a group of lavas that date between 1250 BC and 250 AD, a period that includes the occurrence of a reported intensity high in the Levant

(Gallet et al., 2006; Ben-Yosef et al., 2009; Shaar et al., 2011; Ertepinar et al., 2012). A proper paleointensity record for the Canary Islands for the same period may provide important spatial and temporal constraints for this intriguing, yet enigmatic geomagnetic phenomenon.

Our results will also assess the veracity of the multi-method paleointensity approach for a different volcanic edifice beyond the suite of Hawaiian lavas used in de Groot et al. (2013). For Hawaii it yielded reliable paleointensity estimates for 67% of all cooling units sampled, but its performance for other volcanic regions is yet to be tested. An important part of the multi-method paleointensity approach, the calibrated pseudo-Thellier method, is also used in a different region for the first time. By comparing our pseudo-Thellier results to results of other paleointensity techniques from the same flow, we improve the calibration relation for the pseudo-Thellier technique – although the difference with the calibration relation presented in de Groot et al. (2013) is small. By adding results from a different volcanic edifice to the calibration data the general applicability of the pseudo-Thellier technique to obtain absolute paleointensity estimates for samples that fail in classical techniques due to thermally induced alteration is further enhanced.

2. Geological setting & sampling

The geological history of Tenerife (28° 16' N, 16° 38' W) is mainly dominated by the evolution of two stratovolcanos: Teide and Pico Viejo. The volcanological evolution of the island of Tenerife has been studied in detail (e.g. Carracedo, 1994; Guillou et al., 2004; Carracedo et al., 2007). Numerous Holocene lava flows are present; the most recent volcanic activity is in the Northwest rift zone, in the Chio and Garachico volcanic chains. The island of Gran Canaria (27° 58' N, 15° 35' W) is approximately 100 kms to the East of Tenerife and is somewhat older in geological terms. Gran Canaria is in its post-erosional stage, and active volcanism is much less prominent than on Tenerife. Holocene volcanic activity is limited to the Northeast part of the island, the most recent eruption occurred 200 years ago (Rodriguez-Gonzalez et al., 2009).

For Tenerife, Carracedo et al. (2007) recently presented a suite of both ^{14}C and K/Ar datings from which we selected the nine most recent flows for our study: the oldest flow is ~6000 years old. From the radiocarbon datings for Gran Canaria that were presented by Rodriguez-Gonzalez et al. (2009), we could sample six independent cooling units; some of the dated flows could not be located unambiguously based on the locations provided. A total of 19 independent cooling units were sampled, including four flows dated from historical records (1492, 1706, 1798 and 1909 AD). Some cooling units were sampled at multiple locations (Table 1). Since the laboratory ages are available (Carracedo et al., 2007; Rodriguez-Gonzalez et al., 2009), it was possible to recalibrate the radiocarbon results using the newest INTCAL.13 curve (Reimer et al., 2013) using the Calib 7.0 program (Stuiver and Reimer, 1993). A kml-file with our sampling locations is available in the online Supplementary information.

Samples were usually taken within meters of the given UTM locations (Carracedo et al., 2007; Rodriguez-Gonzalez et al., 2009). Sampling was done using a petrol-powered drill with a bore of 2.5 cm. Taking cores in-situ was not always possible; in those cases (unoriented) hand-samples were taken – paleomagnetic directions are therefore not available for those sites. For each site up to 20 cores were drilled close together to ensure homogeneity between samples since sister specimens are indispensible to compare paleointensity methods. Where possible samples were taken from fresh surfaces (i.e. road cuts) and from solid parts of the flow; sometimes these solid parts were quite vesicular. Two sites, TF-11 and TF-13B, were difficult to drill and appeared to be volcanic glass, implying a rapid natural cooling.

Paleointensity studies on Canary Islands' lavas generally concentrate on pre-Holocene geomagnetic features such as the Matuyama-Brunhes transition; or the Laschamps, Blake, or Mono Lake excursions (e.g. Quidelleur, 1996; Széréméta et al., 1999; Valet et al., 1999; Leonhardt et al., 2000; Leonhardt, 2002; Ferk et al., 2011; Kissel et al., 2011). Studies on Holocene lavas are sparse (Sherwood, 1991; Tulloch, 1992) and only performed on lavas younger than 1435 AD. Two of the

flows presented here were also subject of a study by Valet and Soler (1999), measuring the local field anomalies caused by the morphology of the terrain underneath the cooling lava (Valet and Soler, 1999). Large possible anomalies were reported: the NRM of samples was biased up to 9° in declination, 6.5° in inclination and 20% in intensity, especially near sharp edges in the terrain and close to the underlying flow. The influence of these local field anomalies on the magnetic vector recorded in the flows is reduced by sampling in the upper part of undisturbed large blocks of the cooling units.

3. Rock-magnetic behavior

To optimize the boundary conditions of the paleointensity experiments the rock-magnetic behavior of samples from all sites is characterized first. Both the thermal behavior of the susceptibility and high-field rock-magnetic properties are assessed.

3.1. Susceptibility-versus-temperature (χ-T) analysis

The susceptibility of samples from all sites was measured as function of temperature using an AGICO KLY-3S susceptometer with a CS3 furnace attachment. The temperature was increased in seven cycles with the following approximate peak temperatures: 210, 280, 330, 375, 430, 480 and 580 °C. To check the reversibility of the signal the sample was cooled ~50 °C after reaching each peak temperature. An irreversible susceptibility segment indicates (chemical) alteration in the sample. The highest peak temperature for which the susceptibility still is reversible is the highest temperature that can safely be used in paleointensity experiments, since alteration prevents a reliable paleointensity estimate. Furthermore, the Curie temperature of the samples is obtained from the χ-T diagrams. The Curie temperature is defined here as the inflection point after a peak in susceptibility. Several samples show two or more inflection points, indicating the presence of at least two magnetic carriers with different mineralogical composition. Since the χ-T behavior is diagnostic concerning the magnetic mineral composition and magnetic properties of the samples, the sites are categorized based on this parameter. The boundary conditions of the paleointensity experiments are chosen accordingly.

3.1.1. Group L

Samples that lose 80% of their susceptibility at room-temperature before reaching 150 °C, are labeled as 'type L' (low temperature). Sites TF-2, TF-5, GC-47A, TF-1909A, and the GC-6-(sub-)sites are in this group (Fig. 1b). These sites with a Curie temperature between 100 and 200 °C are vulnerable to viscous overprints. However, the sample shown here retains half of its NRM at 500 °C. The onset of alteration, indicated by non-reversible behavior in the susceptibility-versus-temperature diagram, is generally at 300 – 350 °C. Higher temperature steps in the paleointensity experiments may therefore be not reliable.

3.1.2. Group L*

Samples in group L that show a rapid decay in susceptibility already from room-temperature onwards, interpreted to imply a Hopkinson peak with its related Curie temperature below room-temperature, are labeled 'L*'. All TF-1798 and GC-64-(sub-)sites, and sites GC-73, GC-60, GC-47B and TF-1909B form this group (Fig. 2a). These samples loose approximately half of their NRM after a 100 °C demagnetization step; this makes these samples prone to viscous overprints, since only a small increase in ambient temperature easily reached during drilling, transport or handling the samples can reset part of the NRM. The Zijderveld diagram of the example (Fig. 1a) reveals a slight overprint until 200 °C and is remarkably linear for higher temperatures. The suitability for paleointensity experiments of this group is therefore doubted.

3.1.3. Group H

Group H (high temperature, Fig. 1c) consists of sites TF-9A, TF-9B, TF-14, TF-1706, GC-13, and GC-45; their samples retain more than 80% of their room-temperature susceptibility above 400 °C. These samples are characterized by a relatively constant susceptibility until they lose almost all susceptibility between 500 and 550 °C. The Curie temperature is well expressed at ~520 °C. The samples unblock approximately 25% of their NRM above the 450 °C demagnetization step, with remarkably linear demagnetization behavior. However, the onset of alteration is around 350 °C, well before the Curie

temperature is reached. This implies that obtaining a reliable paleointensity from these samples using thermal methods might prove to be difficult.

3.1.4. Group M

The samples with behavior in-between groups L and H are labeled 'type M', being either a combination of minerals with various dominant Curie temperatures, or a single mineral dominated composition with a broad suite of intermediate Curie temperatures (Dunlop and Özdemir, 1997). This group is formed by sites TF-3, TF-4, TF-6A, TF-6B, TF-13A and TF-1492. The χ-T curves are dominated by at least two Curie temperatures, the lower is generally between 150 and 200 °C. The higher Curie temperature is more difficult to determine because alteration is indicated from approximately 380–450 °C onwards (Fig. 1e). Group M samples unblock up to 60% of their NRM before reaching the alteration temperatures, and show no signs of viscous overprints; therefore these sites should be suitable for paleointensity experiments.

3.1.4. Group M*

The two sites that in the field appeared to be volcanic glass, sites TF-11 and -13B show type M behavior with a Hopkinson peak at approximately 200 °C and a very gradual linear decay of the susceptibility towards 600 °C. They are labeled as rock-magnetic group M* (Fig. 2d). These samples are very dark and glassy and were difficult to sample. Their rock-magnetic behavior is identical and seems very suitable for paleointensity experiments: i.e. the NRM is gradually unblocked between ~200 and 500 °C and there are no signs of alteration up to at least 500 °C.

3.2. High-field rock-magnetic analyses

To assess the magnetic grain size distribution of the samples hysteresis experiments were done and visualized in a Day plot (Day et al., 1977). Per site, three to six tiny specimens (2-10 mg) are used for the determination of the four required parameters. By measuring a hysteresis loop and a backfield curve on a Princeton instruments alternating gradient force magnetometer (PMC Model 2900) the saturation magnetization (M_s), saturation remanent magnetization (M_r), coercive field (B_c) and remanent coercive force (B_{cr}) are obtained. Samples

appeared to be entirely saturated in fields of 0.8 T; the hysteresis loops were corrected for the paramagnetic contribution by the slope between 0.8 and 1 T.

The rock-magnetic groups as defined above do not exhibit systematic behavior in the Day plot (Fig. 1f). The grain size (that dominates the Day plot) and the chemical composition (dominating the χ-T diagrams) do therefore not seem to be correlated. All samples are in the PSD domain, with about one-third of the samples plotting on the theoretical SD+MD mixing lines of magnetite (Dunlop, 2002).

4. Paleomagnetic directions

For each (sub-)site three or four samples were thermally demagnetized using an ASC TD48-SC thermal demagnetizer, magnetizations were measured on a 2G DC-SQUID magnetometer. In 11 steps of 50 °C the samples were demagnetized until only a few percent of the NRM was left at 550 °C. Furthermore, 5-10 samples per site were subjected to an AF demagnetization experiment using a robotized 2G DC-SQUID magnetometer; the peak fields used are 2.5, 5, 7.5, 10, 15, 20, 25, 30, 40, 50, 60, 70, 80, 100, and 150 mT.

We took oriented cores for 11 cooling units; reliable paleodirections can be obtained from these. The directions per cooling unit were averaged using Fisher statistics (results from sub-sites from the same cooling unit were taken together); for each cooling unit 5 to 34 independent sample directions could be interpreted (Table 2). Site means have small values of α_{95}, and k values well above 100, in line with the expected behavior for lavas. Site GC-47, however, has a k value of only 5.6; this direction is therefore rejected. Both declination and inclination of most sites are within the secular variation range expected for their latitude. The declinations of sites TF-4 (~722 BC) and TF-1909A (1909 AD) deviate considerably from true North: 35.7 and -27.0°, respectively.

5. Paleointensities

5.1 Demagnetization behavior

In both IZZI-Thellier and MSP-style paleointensity experiments, the NRM is replaced by pTRMs imparted in a laboratory furnace. The thermal demagnetization behavior of the samples is therefore important to select suitable temperature steps for IZZI-Thellier style experiments and potential set temperatures for MSP-style experiments. In both the thermal and AF demagnetization experiments samples from most sites show univectorial behavior towards the origin (Fig. 1). Sites in rock-magnetic group L* and samples from sites TF-2 and -5 show (viscous) overprints. A viscous overprint makes samples unsuitable for MSP-style experiments since these samples cannot be unambiguously aligned with their NRM in the direction of the applied field during the experiment. In both the IZZI- and pseudo-Thellier experiments, measurements made below the temperature or AF field needed to remove the overprint cannot be faithfully interpreted.

5.2. IZZI-Thellier

The Thellier-Thellier-family of paleointensity measurements is the classical approach in obtaining absolute estimates of the intensity of the geomagnetic field. After its introduction in 1959, several refinements to the protocol were proposed and reliability checks were introduced. In a Thellier-Thellier-experiment the NRM in the samples is progressively replaced by pTRMs due to a series of heating steps to increasingly higher temperatures, alternating between applying a magnetic field in the furnace and not. We subjected at least three samples per site to the IZZI-Thellier paleointensity protocol (Tauxe and Staudigel, 2004) totalling 132 samples altogether. The temperature steps were optimized based on the rock-magnetic groups: for samples with a low Curie temperature more steps were used at low temperatures whereas for samples with a higher Curie temperature, more steps were made to higher temperatures. Both pTRM-checks (Coe, 1967) and tail-checks (Riisager and Riisager, 2001) were performed after every other temperature step. The magnetization of the samples was measured on a 2G DC-SQUID magnetometer; an ASC TD48-SC

thermal demagnetizer was used to demagnetize the samples and impart the pTRMs. The data was interpreted using ThellierTool 4.2 (Leonhardt et al., 2004); some parameters (e.g. $DRAT_{tail}$) must be derived from the ThellierTool output, as these are not produced by the program.

To assess the quality of the IZZI-Thellier results, we used four different sets of selection criteria: TTA and TTB (Leonhardt et al., 2004), SELCRIT-1 (Selkin and Tauxe, 2000) and CLASS-A (de Groot et al., 2014) (Table 3). These sets of selection criteria rely on a number of parameters that describe the quality of Thellier results. These parameters were recently made formally consistent by Paterson et al. (2014) in the 'Standard Paleointensity Definitions', to which we adhere. The performance of the first three sets of selection criteria was assessed in the same study and some modifications to the original criteria were proposed (Paterson et al., 2014), here we use these modified criteria. The fourth set, CLASS-A, focuses on the number of data points ($N \geq 7$) and NRM fraction ($f \geq 0.7$) to be used for the linear fit in the Arai plot (de Groot et al., 2014).

From our 132 samples we obtained 31 results that satisfy at least one of the sets of selection criteria (Fig. 2., Table 3). For a reliable IZZI-Thellier average from a single cooling unit we require at least three successful samples with a standard error that is less than 20% of their mean; such an average could be calculated for sites GC-6, TF-3, TF-4, TF-6, TF-11, and TF-13. The paleointensities of sites that date between 1187 and 723 BC and around 0 AD are high for this latitude: 54.4 ± 3.1 μT (GC-6, 1187 BC), 68.7 ± 2.6 μT (TF-4, 723 BC), 59.6 ± 1.3 μT (TF-11, 42 BC), and 65.7 ± 5.7 μT (TF-3, 74 AD). For two older sites the paleointensities compare well to the current geomagnetic field intensity at the Canary Islands (38.6 μT): 40.9 ± 2.4 μT (TF-6, 1995 BC), and 36.0 ± 4.8 μT (TF-13, 3560 BC). The details of all accepted IZZI-Thellier results are in Supplementary Table S1.

5.3. Microwave-Thellier

Samples from five flows (TF-2, TF-4, TF-5, GC-6, and GC-64) were subjected to the IZZI or the perpendicular (Kono and Ueno, 1977) Thellier protocol using the microwave system at the University of Liverpool (Hill and Shaw, 1999; 2000). A

total of 28 samples could be measured reliably, of which 14 passed at least one of the sets of selection criteria as specified above (Fig. 2, Table 3). For most samples the technical quality of the microwave results surpassed the quality of the thermal results. To accept an average result for a site, we again require at least three successful results with a standard error < 20% of its mean. This yields 56.9 ±5.5 μT for GC-6C; 81.5 ± 2.1 μT for TF-2; 63.9 ± 7.6 μT for TF-4; and 57.3 ± 11.3 μT for TF-5. The details of all microwave Thellier measurements are in Supplementary Table S2.

5.4. MSP-DSC

Where Thellier-style protocols assess pTRMs imparted by a constant laboratory field as function of temperature; multispecimen-style (MSP) experiments assess pTRMs imparted at a constant temperature as function of the laboratory field applied (Dekkers and Böhnel, 2006). In MSP experiments the number of heating steps per sample is considerably lower than in Thellier-style experiments; therefore the risk of magnetic memory effects that might obscure the determination of a reliable paleointensity is reduced. A drawback of this method is that the samples need to be aligned with their NRM in the direction of the applied field in the furnace; this implies that the samples cannot be affected by even small (viscous) overprints. The original MSP protocol as introduced in 2006 did not correct for potential tail or domain state effects; to this end (Fabian and Leonhardt, 2010) proposed an domain state corrected (MSP-DSC) protocol – adding three extra heating steps per sample. The 'α-parameter' in the MSP-DSC analysis was set to 0.5, as suggested by Fabian and Leonhardt (2010).

For all sites in this study up to three potential set temperatures for the MSP-DSC experiments were selected based on the thermal NRM decay curves and alteration temperatures indicated by the χ-T measurements. Ideally, samples should unblock a large part of their NRM before reaching their alteration temperature; and the potential set temperature must be below the 'alteration temperature'. De Groot et al. (2012), however, showed that not all alteration effects are revealed by the χ-T analyses. Very subtle 'magnetic' alteration (explained as transdomain changes) occurring while imparting the pTRMs

prevents a reliable assessment of the paleointensity for some samples. Whether or not such alteration occurs at the set temperature can be assessed prior to paleointensity experiments by an 'ARM-test' (de Groot et al., 2012), which compares anhysteretic remanent magnetization (ARM) acquisition curves of pristine samples to ARM acquisition curves of sister specimens that were heated to the potential set temperature. Ideally, the ARM acquisition behavior is equal for the pristine group of samples and their heated counterparts; different behavior is associated with unreliable paleointensity results at the tested temperature.

After selecting one or more potential set temperatures per site, the single-core variant of the ARM-test was done for various temperatures distributed over all flows. From the 40 ARM-tests, 18 show no or very little alteration after heating. For these 18 site-temperature combinations, the MSP-DSC experiments were done using generally 8-10 samples per experiment – the amount of material permitting. For sites GC-6D and –E the amount of material did unfortunately not allow for ARM-tests; they are both subjected to MSP-DSC experiments at two different temperatures without verification by an ARM-test.

Individual samples that alter more than ±5% during the experiment (i.e. $|\varepsilon_{alt}| > 5\%$) are rejected from the interpretation and an MSP-DSC result is only accepted if the average alteration of the accepted samples is less than ±3%. This rejects seven results. Furthermore, the y-axis intercept of the linear fit must be within 10% of the theoretically predicted -1 (Fabian and Leonhardt, 2010), rejecting another seven results. This leaves six acceptable MSP-DSC results. Four of those are from sub-sites of GC-6 and were interpreted together to yield a paleointensity of 47.7 μT with a standard deviation envelope of 44.0 – 51.5. The other two successful MSP-DSC results are from sites TF-11 and GC-73: 50.6 [45.4-55.6] and 52.8 [51.3-54.5] μT, respectively (Fig. 3, Table 3). The details of all MSP-DSC experiments are in Supplementary Table S3.

5.3. Pseudo-Thellier

It was recently shown that a newly calibrated relative paleointensity technique, the pseudo-Thellier method (Tauxe et al., 1995), is a valuable addition to the toolbox of absolute paleointensity techniques providing estimates of the paleointensity for sites that fail in heating experiments (de Groot et al., 2013). Relative paleointensity techniques are frequently used on sediments and can be obtained either by normalizing the NRM using an ARM or IRM normalizer, or by using the more elaborate pseudo-Thellier approach (Tauxe et al., 1995). These magnetic-mineral-concentration normalizing methods compare the NRM of the samples to laboratory magnetizations that are imparted using alternating or high DC magnetic fields. Importantly, the samples need not to be heated during the experiments. In case of lavas, thermal alteration effects that are known to prevent a reliable estimate of the paleointensity would be avoided; in many studies up to ~80% of the absolute paleointensity experiments done are affected by thermochemical alteration. Yu et al. (2003) explored the potential of using the pseudo-Thellier approach on lavas; he reported a strong grain-size dependence of the obtained results. Since grain sizes in a suite of lavas can range from SD to large MD grains, the pseudo-Thellier method cannot be used straightforwardly to obtain a relative paleointensity curve from such a set of lavas. However, de Groot et al. (2013) proposed a grain-size selector for which the pseudo-Thellier method does yield a reliable relative paleointensity record for lavas meeting the selection criterion. This grain-size selector, the alternating field that imparts half of the saturated ARM in a sample ($B_{½ARM}$), can be obtained directly from the pseudo-Thellier experiments; samples with a $B_{½ARM}$ between 23 and 63 mT are accepted. For samples passing this selection criterion the relative paleointensities can be calibrated to absolute paleointensities using the empirical formula proposed by de Groot et al. (2013).

The first step in a pseudo-Thellier experiment is to AF demagnetize the NRM of 5-10 samples per site; here 165 samples were processed. In 17 steps the NRM of the samples is demagnetized to 300 mT leaving only a few percent of its initial magnitude. The fields used are: 2.5, 5, 7.5, 10, 15, 20, 25, 30, 40, 50, 60, 70, 80, 100, 150, 225 and 300 mT. The fields up to 100 mT are applied by a robotized 2G DC-SQUID magnetometer system that also measures the magnetizations. The

three higher fields are applied in a custom-built demagnetization coil and measured on the same robotized magnetometer. For the second step of the pseudo-Thellier protocol, (p)ARMs are imparted in the samples using the same set of AF field steps as for the demagnetization part of the experiment (step 1). The imparting DC field is set to 40 μT. Between the 225 and 300 mT AF treatments, the ARM generally increases less than 3%, the ARM imparted by 300 mT is therefore regarded as the saturated ARM. The third step in the pseudo-Thellier experiment is to demagnetize the ARM in the samples using the same AF steps as in the first two steps of the pseudo-Thellier protocol.

To obtain a reliable pseudo-Thellier result the (p)ARMs should be carried by the same grains that carried the NRM in the samples. Therefore the demagnetization steps of the NRM (step 1) are plotted against the demagnetization steps of the ARM (step 3). If the same grains carry the NRM and the ARM, the demagnetization behavior of the two should be proportional and therefore linear towards the origin if the NRM of the sample was fully demagnetized (Fig. 4a). The pseudo-Thellier Arai diagrams are interpreted for the AF segment that shows such behavior, generally between 10 and 100 mT. For each specimen the absolute slope of the linear fit in the Arai diagrams (ARM acquired versus NRM remaining, Fig. 4b) and the $B_{½ARM}$ are calculated. The pseudo-Thellier results for samples with a $B_{½ARM}$ between 23 and 63 mT, passing the selection criterion, are grouped to their age. If an age group consists of three or more pseudo-Thellier results, these results are averaged and a standard error is calculated. These averages per age group are then converted to absolute paleointensity estimates using the empirical formula of de Groot et al.: B_{abs} = 7.371 × pseudo-Thellier slope + 14.661 μT (under the premise that the DC-bias field used in the ARM acquisitions is set to 40 μT).

The proposed calibration relation, however, was derived from a suite of Hawaiian lavas and its applicability to other volcanic edifices was unknown. The rock-magnetic group L*, that is abundant on the Canary Islands was not present in the suite of Hawaiian lavas from which the calibration relation was obtained. Since it is very likely that the pseudo-Thellier behavior of lavas not only depends

446 on the grain size distribution as put forward by Yu et al. (2003), but also on the
447 chemical composition of the remanence carrying minerals, we choose not to
448 accept pseudo-Thellier results derived from this rock-magnetic group. Their
449 results are reported merely to assess the performance of this rock-magnetic
450 group as discussed below.
451
452 Furthermore, the calibration relation was based on a relatively small range of
453 intensities and the results from samples with paleointensities between 35 and
454 40 μT were extrapolated to the higher paleointensities present in the Hawaiian
455 data set. We now compare the pseudo-Thellier results of sites with higher
456 paleointensities (up to 80 μT) to results of thermal paleointensity techniques
457 obtained from the same sites in both the Hawaiian and Canary Islands data set
458 (Fig. 5). The linear regression through all data provides an improved calibration
459 relation to convert pseudo-Thellier data into absolute paleointensity estimates:
460 B_{abs} = 7.944 × pseudo-Thellier slope + 13.789 μT (with the DC-bias field used in
461 the ARM acquisitions set to 40 μT). The calibration relation in de Groot et al.
462 (2013) is well within the 95% confidence interval of the updated relation, and
463 differences between the outcomes of the two relations are <5% for typical
464 paleointensities. The updated calibration relation, however, is supported by a
465 broader range of paleointensities elucidating the general applicability of the
466 pseudo-Thellier method for these fields. Data for units that cooled in a lower
467 Earth's magnetic field are unfortunately not available; the problem of the non-
468 zero y-axis intercept (de Groot et al., 2013) can therefore not be resolved by the
469 available data.
470
471 From the 165 samples subjected to the pseudo-Thellier protocol, 49 exhibit a
472 $B_{½ARM}$ between 23 and 63 mT. With at least three samples per site/age, this
473 yields pseudo-Thellier estimates (using the improved calibration relation) for
474 nine sites (TF-2, TF-4, TF-5, TF-6, TF-14, TF-1706, TF-1909; GC-6, and GC-47).
475 For seven of these sites, the pseudo-Thellier averages are derived from samples
476 from rock-magnetic groups L, M, and/or H; three of these (TF-6, -14 and -1706)
477 yield paleointensity estimates between 35 and 40 μT; the paleointensities of the
478 other four (TF-2, TF-4, TF-5, and GC-6) are notably high: 81.6, 62.2, 58.6, and

52.3 μT, respectively (Table 3). The pseudo-Thellier averages for the two remaining sites are derived from samples from rock-magnetic group L* and are not accepted as reliable paleointensity estimates; they yield: 21.7 and 45.5 μT for sites TF-1909 and GC-47, respectively. The details of all pseudo-Thellier samples and averages are included in Supplementary Tables S4 and S5.

6. Discussion

6.1. Comparing paleointensity methods and materials

By using four methods in one paleointensity study and interpreting the results using predefined selection criteria, the success rate in obtaining reliable paleointensities from lavas can be significantly increased. With our multi-method paleointensity approach we obtained a reliable paleointensity estimate for 11 out of 19 dated flows, a success rate of almost 60%. This compares well to the success rate on Hawaiian lavas: 67% (de Groot et al., 2013). The success rates of the four methods individually are only 32% (IZZI-Thellier), 21% (Microwave-Thellier), 16% (MSP-DSC), and 37% (pseudo-Thellier). For five sites only one of the applied methods was successful, for the other six at least two methods yielded a reliable paleointensity estimate. All four methods were successful in only one site (GC-6). Differences in the results from various methods are generally small: often the estimates are within each other's confidence interval and/or differ less than 10% (Table 3). If a paleointensity estimate can be confirmed using two or more methods, the credibility of these results is considerably enhanced (de Groot et al., 2013; Biggin and Patterson, 2014).

For site GC-6, all four methods yielded reliable results although the thermal and microwave Thellier results are somewhat higher than the results of the MSP-DSC and pseudo-Thellier methods. This might be explained by variations in the three sub-sites of GC-6: the thermal- and microwave-Thellier averages are dominated by samples from GC-6C and –D, while only samples from GC-6E could be interpreted for the pseudo-Thellier estimate; the MSP-DSC result is an average of all three sub-sites. The difference between the IZZI-Thellier and MSP-DSC result

of site TF-11 (59.9 and 50.6 μT, respectively) is harder to explain: both experiments easily pass the selection criteria applied.

Samples with different rock-magnetic behavior are successful in certain paleointensity experiments, but fail in others. Samples from rock-magnetic group H are unsuccessful in thermal paleointensity experiments, but two out of three sites yield reliable pseudo-Thellier results. This can be explained by the onset of thermally induced alteration before a considerable portion of the NRM of the samples is unblocked, which is avoided in the pseudo-Thellier experiments. The IZZI-Thellier method generally works well for rock-magnetic groups M and M*, with five out of eight flows yielding a reliable estimate. The microwave yielded good results for samples from rock-magnetic group L: all three sites tried yielded a proper paleointensity estimate. Since lava flows are generally not homogeneous in terms of rock-magnetic properties (e.g. Biggin et al., 2007; de Groot et al., 2014), the chances of obtaining a reliable paleointensity estimate for a particular age can be further increased by sampling one cooling unit at multiple locations – although this may in practice not always be feasible; e.g. because of restrictions in the terrain and the availability of (radiocarbon) datings.

6.2. The veracity of the calibrated pseudo-Thellier method

All pseudo-Thellier results derived from rock-magnetic groups L, M and H compare well to results from other (thermal) paleointensity techniques for the same sites – i.e. the differences between the pseudo-Thellier results and the other paleointensities are not larger than the mutual variation in the results of other paleointensity methods per site (Table 3). For rock-magnetic group L*, however, the pseudo-Thellier results are lower than expected. Site TF-1909 yielded 22.0 μT, approximately half of the expected value for 1909 AD; and the value found for GC-47 is on average ~15% lower than the paleointensities obtained from a site that is only ~80 years younger (GC-6) – while an increase in paleointensity is expected in that period. Since the ARM characteristics of samples not only depend on grain size (Yu et al., 2003), but also on chemical composition (e.g. Dunlop and Özdemir, 1997), it is very likely that the calibration relation also depends on the chemistry of the remanence carrying minerals –

assessed here by their bulk χ-T behavior. This is not considered in the current calibration relation that is, in fact, surprisingly tolerant in grain size distribution accepted (i.e. the width of the $B_{½ARM}$-window). Here we emphasize that the chemical composition must also be considered to select samples for the pseudo-Thellier methods. Currently it is best to disregard samples from rock-magnetic group L*, but in a future stage –when measurements from more sites with varying rock-magnetic and grain-size distributions become available– both the grain-size dependence and the chemical composition of the samples may be considered in an updated pseudo-Thellier calibration.

6.3. Compiling the full vector record

The obtained paleodirections and –intensities can now be compiled together with existing data into a full vector record for the Canary Islands (Fig. 6). The resolution of this record, and therefore its fidelity, is governed by the availability of well-dated lava flows. For the declination and inclination two recent geomagnetic models PFM9K.1b (Nilsson et al., 2014) and SHA.DIF.14k (Pavón-Carrasco et al., 2014) coincide well with most of our findings. The models also match some intensity data, but especially the SHA.DIF.14k model predicts lower values than we found for the period between ~1500 BC to 250 AD.

6.4. Dating of site TF-2

The highest paleointensity reported here is ~80 μT (corresponding to a VADM of ~160 ZAm^2) for a flow that is dated at 1058 AD (Carracedo et al., 2007). Our estimate obtained from two independent paleointensity methods differs approximately 70 ZAm^2 from at least 10 coeval VADMs reported by three different studies within a 2000 km radius (Fig. 7a); and its inclination is more than 20 ° steeper than expected based on geomagnetic models (Nilsson et al., 2014 ; Pavón-Carrasco et al., 2014)(Fig. 6). Furthermore, its paleomagnetic direction is close to the paleomagnetic direction of site GC-60 (612 BC) and would match the geomagnetic models between ~400-300 BC (Fig. 6: the declination matches between ~400-300 BC; the inclination matches between ~700-100 BC, especially with the SHA.DIF.14k model). This paleomagnetic dating would place the high paleointensity values in a more plausible time frame considering the high paleointensities found for sites between ~1000 BC – 100

AD. The radiocarbon that was dated and associated with this flow was found just beneath the flow in a trench on the edge of what is now a pine forest (Carracedo et al., 2007). Since we did not carry out the dating ourselves it is hard to assess whether it is possible that a younger piece of carbon (e.g. as a result of a forest fire) became enclosed in the soil that was dated. We emphasize that there is no further evidence to disregard the radiocarbon dating besides the paleomagnetic correlation above; our alternative interpretation is therefore rather tentative.

6.5. Spatial and temporal extent of the Levant intensity high

We selected a number of lavas dating between 1250 BC and 250 AD to assess the spatial and temporal extent of the Levant intensity high (Genevey et al., 2003; Gallet et al., 2006; Ben-Yosef et al., 2009; Shaar et al., 2011; Ertepinar et al., 2012). We find high paleointensities for approximately the same period (Fig. 7b), although the mean VADMs per site are consistently below the 10-point moving average through the Levant-data – at least until 723 BC. For the period between ~1050–500 BC, paleointensity data from other parts of the world are sparse; for Mexico VADMs of ~82 (Pétronille et al., 2012) and ~105 ZAm^2 (Duran et al., 2010) are suggested and Yu (2012) and Hong et al. (2013) report VADMs of ~80-90 ZAm^2 for Japan and South Korea, respectively, around ~750 BC . All reported values are much lower than the values reported for the Middle East (>150 ZAm^2) and the Canary Islands (~125 ZAm^2). Although the geomagnetic dipole was relatively high around 1000 BC (e.g. Hong et al., 2013), the large synchronous differences between various locations on Earth cannot sustain a dipolar explanation of the Levant intensity high. Furthermore, the VADMs reported for the Levant exceed the dipole contributions to geomagnetic field models by 50% (Korte et al., 2011); the Levant intensity high must therefore be explained by higher order contributions, like the intensity highs reported between 400 AD and today (de Groot et al., 2013). Nevertheless we notice that the spatial influence of this geomagnetic trait is quite large – the Levant and the Canary Islands are at approximately the same latitude, but differ 50-60° in longitude.

To further constrain the Levant intensity high in space and time, the dating of site TF-2 is critical. Its VADM of ~160 ZAm^2 compares well with the 10-point

moving average for the Levant ~1000 BC. Based on its paleomagnetic direction, however, TF-2 would be dated to ~400-300 BC. The intensity peak in the Canary Islands would then occur considerably later than in the Levant, implying a westward motion of this phenomenon. A compilation of geomagnetic data for the Balkan region (Tema and Kondopoulou, 2011), shows a less prominent peak (up to 125 ZAm^2) that post-dates the Levant intensity high by ~500 years. The confidence intervals (both in time and paleointensity) associated with this record, however, is quite large; and the Balkan is relatively far to the North compared to the Levant and the Canary Islands. Directional variations for the Levant, Balkan, and Canary Islands regions further substantiate a westward motion of the Levant intensity high. During the peak in paleointensities in the Levant, the declinations for the Middle East are approximately true North (Ertepinar et al., 2012); while the declination at Tenerife is up to ~20-35° to the East, this is in good agreement with both the Spanish (Gómez-Paccard et al., 2006a) and British (Zananiri et al., 2007) secular variation master curves. Around ~500 BC, the declination in the Canary Islands is approximately true North, while the declination for the Levant is more than 10 degrees to the West. The declination curve for the Balkan – that is better constrained than the intensity curve - shows a change from ~15 degrees East (deviated towards the longitude of the Levant) to 15 degrees West (deviated towards the Canary Islands longitude) (Tema and Kondopoulou, 2011). We therefore hypothesize that the observed behavior may be explained by a regional field anomaly produced by a strong non-dipole field centered in the Levant around ~1000 BC and moving to the west at a rate of 6.7-12.0° per century.

7. Conclusion

The multi-method paleointensity approach yielded reliable estimates of the paleointensity for ~60% of all cooling units sampled in this study. This testifies to its potential to obtain high-resolution intensity records from volcanic edifices and its applicability to other volcanic areas beyond Hawaii. A further assessment of the calibrated pseudo-Thellier method corroborates its potential to provide absolute paleointensity estimates for sites that suffer from thermally induced

alteration during traditional, thermal paleointensity techniques. Our new record for the Canary Islands reveals paleointensities higher than 100 ZAm^2 between ~1250 BC to ~250 AD and provides important constraints for the Levant intensity high. Its influence reached at least 50-60° west, and our data may suggest a westward movement of this geomagnetic phenomenon at a rate of 6.7-12° per century.

Acknowledgements

The late Tom Mullender has been a great help in the laboratory; his interest and support are deeply missed. This research was funded by a grant from the Earth and Life Science Division (ALW) of the Netherlands Organization for Scientific Research (NWO). LVdG acknowledges a grant from the Netherlands Research Center for Integrated Solid Earth Sciences (ISES). AJB acknowledges funding from a NERC Advanced Fellowship (NE/F015208/1).

References

Aitken, M.J., Allsop, A.L., Bussell, G.D., Winter, M.B., 1984. Geomagnetic intensity in Egypt and western Asia during the second millennium BC. Nature 310, 305-306.

Ben-Yosef, E., Ron, H., Tauxe, L., Agnon, A., Genevey, A., Levy, T.E., Avner, U., Najjar, M., 2008. Application of copper slag in geomagnetic archaeointensity research. J. Geophys. Res. 113, B08101. doi:10.1029/2007JB005235

Ben-Yosef, E., Tauxe, L., Levy, T.E., Shaar, R., Ron, H., Najjar, M., 2009. Geomagnetic intensity spike recorded in high resolution slag deposit in Southern Jordan. Earth Planet. Sci. Lett. 287, 529–539. doi:10.1016/j.epsl.2009.09.001

Biggin, A.J., Perrin, M., Dekkers, M.J., 2007. A reliable absolute palaeointensity determination obtained from a non-ideal recorder. Earth Planet. Sci. Lett. 257, 545–563. doi:10.1016/j.epsl.2007.03.017

Biggin, A.J., Paterson, G.A., 2014. A new set of qualitative reliability criteria to aid inferences on palaeomagnetic dipole moment variations through geological time. Front. Earth Sci. 2, 24. doi:10.3389/feart.2014.00024

Carracedo, J.C., 1994. The Canary Islands: an example of structural control on the growth of large oceanic-island volcanoes. J. Volcanol. Geoth. Res. 60, 225–241.

Carracedo, J.C., Badiola, E.R., Guillou, H., Paterne, M., Scaillet, S., Torrado, F.J.P., Paris, R., Fra-Paleo, U., Hansen, A., 2007. Eruptive and structural history of Teide Volcano and rift zones of Tenerife, Canary Islands. Geol. Soc. Am. Bull. 119, 1027–1051. doi:10.1130/B26087.1

Catanzariti, G., Gómez-Paccard, M., McIntosh, G., Pavón-Carrasco, F.J., Chauvin, A., Osete, M.L., 2012. New archaeomagnetic data recovered from the study of Roman and Visigothic remains from central Spain (3rd-7th centuries). Geophys. J. Int. 188, 979–993. doi:10.1111/j.1365-246X.2011.05315.x

Coe, R.S., 1967. Paleo-intensities of the Earth's magnetic field determined from Tertiary and Quaternary rocks. J. Geophys. Res. 72, 3247–3262.

Day, R., Fuller, M., Schmidt, V., 1977. Hysteresis properties of titanomagnetites: grain-size and compositional dependence. Phys. Earth Planet. Inter. 13, 260–267.

de Groot, L.V., Biggin, A.J., Dekkers, M.J., Langereis, C.G., Herrero-Bervera, E., 2013. Rapid regional perturbations to the recent global geomagnetic decay revealed by a new Hawaiian record. Nature Commun. 4, 1–7. doi:10.1038/ncomms3727

de Groot, L.V., Dekkers, M.J., Mullender, T.A.T., 2012. Exploring the potential of acquisition curves of the anhysteretic remanent magnetization as a tool to detect subtle magnetic alteration induced by heating. Phys. Earth Planet. Inter. 194-195, 1–14. doi:10.1016/j.pepi.2012.01.006

de Groot, L.V., Dekkers, M.J., Visscher, M., Maat, ter, G.W., 2014. Magnetic properties and paleointensities as function of depth in a Hawaiian lava flow. Geochem. Geophys. Geosyst. 15. doi:10.1002/2013GC005094

Dekkers, M.J., Böhnel, H.N., 2006. Reliable absolute palaeointensities independent of magnetic domain state. Earth Planet. Sci. Lett. 248, 508–517.

697 doi:10.1016/j.epsl.2006.05.040
698 Di Chiara, A., Tauxe, L., Speranza, F., 2014. Paleointensity determination from São
699 Miguel (Azores Archipelago) over the last 3ka. Phys. Earth Planet. Inter. 234,
700 1–13. doi:10.1016/j.pepi.2014.06.008
701 Donadini, F., Korte, M., Constable, C.G., 2009. Geomagnetic field for 0–3 ka: 1.
702 New data sets for global modeling. Geochem. Geophys. Geosyst. 10, Q06007.
703 doi:10.1029/2008GC002295
704 Dunlop, D.J., 2002. Theory and application of the Day plot (Mrs/Ms versus
705 Hcr/Hc) 1. Theoretical curves and tests using titanomagnetite data. J.
706 Geophys. Res. 107, 2056. doi:10.1029/2001JB000486
707 Dunlop, D.J., Özdemir, Ö., 1997. Cambridge Studies in Magnetism: Rock
708 Magnetism: Fundamentals and Frontiers. Cambridge University Press,
709 Cambridge, UK. 1–1.
710 Duran, M.P., Goguitchaichvili, A., Morales, J., Reyes, B.A., Valdivia, L.M.A., Oliveros-
711 Morales, A., Calvo-Rathert, M., Moran, T.G., Robles-Camacho, J., 2010.
712 Magnetic properties and Archeointensity of Earth's magnetic field recovered
713 from El Opeño, earliest funeral architecture known in Western Mesoamerica.
714 Stud. Geophys. Geod. 54, 575–593.
715 Ertepinar, P., Langereis, C.G., Biggin, A.J., Frangipane, M., Matney, T., Ökse, T.,
716 Engin, A., 2012. Archaeomagnetic study of five mounds from Upper
717 Mesopotamia between 2500 and 700 BCE Further evidence for an extremely
718 strong geomagnetic field ca. 3000 years ago. Earth Planet. Sci. Lett. 357-358,
719 84–98. doi:10.1016/j.epsl.2012.08.039
720 Fabian, K., Leonhardt, R., 2010. Multiple-specimen absolute paleointensity
721 determination: An optimal protocol including pTRM normalization, domain-
722 state correction, and alteration test. Earth Planet. Sci. Lett. 297, 84–94.
723 doi:10.1016/j.epsl.2010.06.006
724 Ferk, A., Leonhardt, R., Aulock, von, F.W., Hess, K.U., Dingwell, D.B., 2011.
725 Paleointensities of phonolitic obsidian: Influence of emplacement rotations
726 and devitrification. J. Geophys. Res. 116, B12113.
727 doi:10.1029/2011JB008397
728 Gallet, Y., Butterlin, P., 2014. Archaeological and Geomagnetic Implications of
729 New Archaeomagnetic Intensity Data from the Early Bronze High Terrace
730 "Massif Rouge"at Mari (Tell Hariri, Syria). Archaeometry.
731 doi:10.1111/arcm.12112
732 Gallet, Y., D'Andrea, M., Genevey, A., Pinnock, F., Le Goff, M., Matthiae, P., 2014.
733 Archaeomagnetism at Ebla (Tell Mardikh, Syria). New data on geomagnetic
734 field intensity variations in the Near East during the Bronze Age. J. Arch. Sci.
735 42, 295–304. doi:10.1016/j.jas.2013.11.007
736 Gallet, Y., Genevey, A., LeGoff, M., Fluteau, F., ALIESHRAGHI, S., 2006. Possible
737 impact of the Earth's magnetic field on the history of ancient civilizations.
738 Earth Planet. Sci. Lett. 246, 17–26. doi:10.1016/j.epsl.2006.04.001
739 Gallet, Y., Le Goff, M., 2006. High-temperature archeointensity measurements
740 from Mesopotamia. Earth And Planetary Science Letters 241, 159–173.
741 doi:10.1016/j.epsl.2005.09.058
742 Genevey, A., Gallet, Y., Margueron, J.C., 2003. Eight thousand years of
743 geomagnetic field intensity variations in the eastern Mediterranean. J.
744 Geophys. Res.: Solid Earth 108. doi:10.1029/2001JB001612
745 Gómez-Paccard, M., Beamud, E., McIntosh, G., Larrasoana, J.C., 2013. New

746 archaeomagnetic data recovered from the study of three Roman kilns from
747 North-East Spain: a contribution to the Iberian palaeosecular variation curve.
748 Archaeometry 55, 159–177. doi:10.1111/j.1475-4754.2012.00675.x
749 Gómez-Paccard, M., Chauvin, A., Lanos, P., Dufresne, P., Kovacheva, M., Hill, M.J.,
750 Beamud, E., Blain, S., Bouvier, A., Guibert, P., Team, A.W., 2012a. Improving
751 our knowledge of rapid geomagnetic field intensity changes observed in
752 Europe between 200 and 1400 AD. Earth Planet. Sci. Lett. 355-356, 131–143.
753 doi:10.1016/j.epsl.2012.08.037
754 Gómez-Paccard, M., Chauvin, A., Lanos, P., McIntosh, G., Osete, M.L., Catanzariti,
755 G., Ruiz-Martínez, V.C., Núñez, J.I., 2006a. First archaeomagnetic secular
756 variation curve for the Iberian Peninsula: Comparison with other data from
757 western Europe and with global geomagnetic field models. Geochem.
758 Geophys. Geosyst. 7, Q12001. doi:10.1029/2006GC001476
759 Gómez-Paccard, M., Chauvin, A., Lanos, P., Thiriot, J., 2008. New archeointensity
760 data from Spain and the geomagnetic dipole moment in western Europe over
761 the past 2000 years. J. Geophys. Res. 113, B09103.
762 doi:10.1029/2008JB005582
763 Gómez-Paccard, M., Chauvin, A., Lanos, P., Thiriot, J., Jiménez-Castillo, P., 2006b.
764 Archeomagnetic study of seven contemporaneous kilns from Murcia (Spain).
765 Phys. Earth Planet. Inter. 157, 16–32. doi:10.1016/j.pepi.2006.03.001
766 Gómez-Paccard, M., McIntosh, G., Chauvin, A., Beamud, E., Pavón-Carrasco, F.J.,
767 Thiriot, J., 2012b. Archaeomagnetic and rock magnetic study of six kilns from
768 North Africa (Tunisia and Morocco). Geophys. J. Int. 189, 169–186.
769 doi:10.1111/j.1365-246X.2011.05335.x
770 Guillou, H., Carracedo, J.C., Paris, R., Pérèz Torrado, F.J., 2004. Implications for the
771 early shield-stage evolution of Tenerife from K/Ar ages and magnetic
772 stratigraphy. Earth Planet. Sci. Lett. 222, 599–614.
773 doi:10.1016/j.epsl.2004.03.012
774 Hartmann, G.A., Trindade, R.I., Goguitchaichvili, A., Etchevarne, C., Morales, J.,
775 Afonso, M.C., 2009. First archeointensity results from Portuguese potteries
776 (1550-1750 AD). Earth Planets Space 61, 93.
777 Hill, M.J., Shaw, J., 1999. Palaeointensity results for historic lavas from Mt Etna
778 using microwave demagnetization/remagnetization in a modifiedThellier-
779 type experiment. Geophys. J. Int. 139, 583–590.
780 Hill, M.J., Shaw, J., 2000. Magnetic field intensity study of the 1960 Kilauea lava
781 flow, Hawaii, using the microwave palaeointensity technique. Geophys. J. Int.
782 142, 487–504.
783 Hong, H., Yu, Y., Lee, C.H., Kim, R.H., Park, J., Doh, S.-J., Kim, W., Sung, H., 2013.
784 Globally strong geomagnetic field intensity circa 3000 years ago. Earth
785 Planet. Sci. Lett. 383, 142–152. doi:10.1016/j.epsl.2013.09.043
786 Kissel, C., Guillou, H., Laj, C., Carracedo, J.C., Nomade, S., Perez-Torrado, F.,
787 Wandres, C., 2011. The Mono Lake excursion recorded in phonolitic lavas
788 from Tenerife (Canary Islands): Paleomagnetic analyses and coupled K/Ar
789 and Ar/Ar dating. Phys. Earth Planet. Inter. 187, 232–244.
790 doi:10.1016/j.pepi.2011.04.014
791 Kissel, C., Rodriguez-Gonzalez, A., Laj, C., Perez-Torrado, F., Carracedo, J.C.,
792 Wandres, C., Guillou, H., 2015. Paleosecular variation of the earth magnetic
793 field at the Canary Islands over the last 15 ka. Earth Planet. Sci. Lett. 412,
794 52–60. doi:10.1016/j.epsl.2014.12.031

795 Kono, M., Ueno, N., 1977. Paleointensity determination by a modified Thellier
796 method. Phys. Earth Planet. Inter. 13, 305–314.
797 Korhonen, K., Donadini, F., Riisager, P., Pesonen, L.J., 2008. GEOMAGIA50: An
798 archeointensity database with PHP and MySQL. Geochem. Geophys. Geosyst.
799 9, Q04029. doi:10.1029/2007GC001893
800 Korte, M., Constable, C., Donadini, F., Holme, R., 2011. Reconstructing the
801 Holocene geomagnetic field. Earth Plan. Sci. Lett. 312, 497–505.
802 doi:10.1016/j.epsl.2011.10.031
803 Leonhardt, R., 2002. A reversal of the Earth's magnetic field recorded in mid-
804 Miocene lava flows of Gran Canaria: Paleointensities. J. Geophys. Res. 107,
805 2299. doi:10.1029/2001JB000949
806 Leonhardt, R., Heunemann, C., Krasa, D., 2004. Analyzing absolute paleointensity
807 determinations: Acceptance criteria and the software ThellierTool4.0.
808 Geochem. Geophys. Geosyst. 5, Q12016. doi:10.1029/2004GC000807
809 Leonhardt, R., Hufenbecher, F., Heider, F., 2000. High absolute paleointensity
810 during a mid Miocene excursion of the Earth's magnetic field. Earth Planet.
811 Sci. Lett. 184, 141–154.
812 Mitra, R., Tauxe, L., McIntosh, S.K., 2013. Two thousand years of archeointensity
813 from West Africa. Earth Planet. Sci. Lett. 364, 123–133.
814 doi:10.1016/j.epsl.2012.12.027
815 Nachasova, I.E., Burakov, K.S., 2009. Variation of the intensity of the Earth's
816 magnetic field in Portugal in the 1st millennium BC. Izv-Phys Solid Earth 45,
817 595–603. doi:10.1134/S1069351309070040
818 Nilsson, A., Holme, R., Korte, M., Suttie, N., Hill, M., 2014. Reconstructing Holocene
819 geomagnetic field variation: new methods, models and implications.
820 Geophys. J. Int. 198, 229–248. doi:10.1093/gji/ggu120
821 Paterson, G.A., Tauxe, L., Biggin, A.J., Shaar, R., Jonestrask, L.C., 2014. On
822 improving the selection of Thellier-type paleointensity data. Geochem.
823 Geophys. Geosyst. 15, 1180–1192. doi:10.1002/2013GC005135
824 Pavón-Carrasco, F.J., Osete, M.L., Torta, J.M., De Santis, A., 2014. A geomagnetic
825 field model for the Holocene based on archaeomagnetic and lava flow data.
826 Earth Planet. Sci. Lett. 388, 98–109. doi:10.1016/j.epsl.2013.11.046
827 Pétronille, M., Goguitchaichvili, A., Morales, J., Carvallo, C., Hueda-Tanabe, Y.,
828 2012. Absolute geomagnetic intensity determinations on Formative
829 potsherds (1400–700 BC) from the Oaxaca Valley, Southwestern Mexico.
830 Quarter. Res. 78, 442–453. doi:10.1016/j.yqres.2012.07.011
831 Quidelleur, X., 1996. Geomagnetic changes across the last reversal recorded in
832 lava flows from La Palma, Canary Islands. J. Geophys. Res. 101, 13755–
833 13733.
834 Reimer, P.J., Bard, E., Bayliss, A., Beck, J.W., Blackwell, P.G., Ramsey, C.B., Buck,
835 C.E., Cheng, H., Edwards, R.L., Friedrich, M., 2013. IntCal13 and Marine13
836 radiocarbon age calibration curves 0–50,000 years cal BP. Radiocarbon 55,
837 1869–1887.
838 Riisager, P., Riisager, J., 2001. Detecting multidomain magnetic grains in Thellier
839 palaeointensity experiments. Phys. Earth Planet. Inter. 125, 111–117.
840 Rodriguez-Gonzalez, A., Fernandez-Turiel, J.L., Perez-Torrado, F.J., Hansen, A.,
841 Aulinas, M., Carracedo, J.C., Gimeno, D., Guillou, H., Paris, R., Paterne, M., 2009.
842 The Holocene volcanic history of Gran Canaria island: implications for
843 volcanic hazards. J. Quaternary Sci. 24, 697–709. doi:10.1002/jqs.1294

844 Selkin, P.A., Tauxe, L., 2000. Long-term variations in palaeointensity. Philos T Roy
845 Soc A 358, 1065–1088.
846 Shaar, R., Ben-Yosef, E., Ron, H., Tauxe, L., Agnon, A., Kessel, R., 2011.
847 Geomagnetic field intensity: How high can it get? How fast can it change?
848 Constraints from Iron Age copper slag. Earth Planet. Sci. Lett. 301, 297–306.
849 doi:10.1016/j.epsl.2010.11.013
850 Sherwood, G.J., 1991. Evaluation of a multi-specimen approach to palaeointensity
851 determination. J. Geomag. Geoelec. 43, 341–349.
852 Stuiver, M., Reimer, P.J., 1993. Extended 14C data base and revised CALIB 3.0 14C
853 age calibration program. Radiocarbon 35, 215–230.
854 Széréméta, N., Laj, C., Guillou, H., Kissel, C., Mazaud, A., Carracedo, J.C., 1999.
855 Geomagnetic paleosecular variation in the Brunhes period, from the island of
856 El Hierro (Canary Islands). Earth Planet. Sci. Lett. 165, 241–253.
857 Tauxe, L., Pick, T., Kok, Y., 1995. Relative paleointensity in sediments: a pseudo-
858 Thellier approach. Geophys. Res. Lett. 22, 2885–2888.
859 Tauxe, L., Staudigel, H., 2004. Strength of the geomagnetic field in the Cretaceous
860 Normal Superchron: New data from submarine basaltic glass of the Troodos
861 Ophiolite. Geochem. Geophys. Geosyst. 5, Q02H06.
862 Tema, E., Kondopoulou, D., 2011. Secular variation of the Earth's magnetic field
863 in the Balkan region during the last eight millennia based on
864 archaeomagnetic data. Geophys. J. Int. 186, 603–614. doi:10.1111/j.1365-
865 246X.2011.05088.x
866 Tulloch, A.M., 1992. Ph.D. Thesis, University of Liverpool.
867 Valet, J.-P., Soler, V., 1999. Magnetic anomalies of lava fields in the Canary islands.
868 Possible consequences for paleomagnetic records. Phys. Earth Planet. Inter.
869 115, 109–118.
870 Valet, J.P., Brassart, J., Quidelleur, X., Soler, V., Gillot, P.-Y., Hongre, L., 1999.
871 Paleointensity variations across the last geomagnetic reversal at La Palma,
872 Canary Islands, Spain. J. Geophys. Res. 104, 7577–7598.
873 Yu, Y., 2012. High-fidelity paleointensity determination from historic volcanoes
874 in Japan. J. Geophys. Res. 117, B08101. doi:10.1029/2012JB009368
875 Yu, Y., Dunlop, D.J., Özdemir, Ö., 2003. Are ARM and TRM analogs? Thellier
876 analysis of ARM and pseudo-Thellier analysis of TRM. Earth Planet. Sci. Lett.
877 205, 325–336.
878 Zananiri, I., Batt, C.M., Lanos, P., Tarling, D.H., Linford, P., 2007. Archaeomagnetic
879 secular variation in the UK during the past 4000 years and its application to
880 archaeomagnetic dating. Phys. Earth Planet. Inter. 160, 97–107.
881 doi:10.1016/j.pepi.2006.08.006
882
883

Captions to figures and tables

Fig. 1 – Paleomagnetic and rock-magnetic analyses. For each rock-magnetic group a typical χ-T diagram and a Zijderveld diagram of a thermal demagnetization experiment are shown: clock-wise, starting in the upper-left corner: rock-magnetic type L* (panels a); type L (panels b); type H (panels c); type M* (panels d); and type M (panels e). For ease of comparison the directions in all Zijderveld diagrams are put to approximately zero declination, and an inclination of ~45° down. In the χ-T plots the different temperature segments have different colors. The Curie temperature can be obtained by the estimating the inflection point after a Hopkinson peak; some samples show multiple inflection points. A non-reversible temperature segment indicates alteration; the maximum temperature in the segment with the highest temperature that still is reversible is regarded as the highest temperature that can be safely utilized in paleointensity experiments. The Day-plot (panel f) (Day et al., 1977) indicates the grain size of the various samples. Samples from rock-magnetic group L are solid orange squares; rock-magnetic group L* open orange squares; group M solid red circles; group M* open red circles; and group H blue triangles. The theoretical mixing lines for the coarse and fine grained end member (Day et al., 1977; Dunlop, 2002) are also indicated (curved dashed lines), the area in between these mixing lines is shaded.

Fig. 2 – Thellier results. Six examples of typical thermal IZZI-Thellier results passing the different sets of selection criteria applied. Data points used in the linear interpolation (blue line) are closed circles, data points disregarded are open circles. Checks are open triangles. Some temperatures are indicated, as well as the site and sample code (between brackets) and the obtained paleointensity (Int.) with its one standard deviation confidence interval. Both axes are normalized to the starting NRM (NRM_0). The sets of selection criteria passed are specified in each panel: S = modified SELCRIT-01 (Selkin and Tauxe, 2000; Biggin et al., 2007; Paterson et al., 2014), TTA = modified ThellierTool A (Leonhardt et al., 2004; Paterson et al., 2014), TTB = modified ThellierTool B (Leonhardt et al., 2004; Paterson et al., 2014), and A = CLASS-A (de Groot et al.,

916 2014). The bottom row (panels g-i) are microwave IZZI results that are generally
917 technically more successful.
918
919 Fig. 3 – MSP-DSC results. The result of site TF-11 is in panel a (data points solid
920 dots, the linear fit is the solid line and the one-standard deviation error envelop
921 is dashed), with its ARM-test in panel c. Site GC-73 (panel b) yielded 5 samples
922 (two indistinguishably close together) that altered more than 5% between step 1
923 and step 4 and were therefore rejected from the interpretation (open circles);
924 the accepted data points are depicted with rescaled axis in the inset. The ARM-
925 test of site GC-73 is in panel e. For site GC-6 ARM-tests are not available due to a
926 limited amount of material, but the MSP-DSC result is based on four different
927 sub-site/temperature combinations all yielding comparable results: sub-site C at
928 150 °C in blue, sub-site D at 150 °C in purple, sub-site D at 200 °C in yellow, and
929 sub-site E at 250 °C in red; one rejected data point is the open dot.
930
931 Fig. 4 – Pseudo-Thellier example (site TF-6B). If the same grains that carried the
932 NRM carry the ARM, the trend in the demagnetization of the NRM versus the
933 demagnetization of the ARM (panel a) should be linear towards the origin (under
934 the premise that the NRM was fully removed). Five different samples are shown
935 in different colors and symbols, the lines are the linear trend-lines through the
936 data in the corresponding color. For low AF fields, the NRM of the samples may
937 suffer from a viscous overprint (grey area in the upper right corner). In this
938 example the overprints are removed by a field of 7.5 mT (open symbols); for
939 very high AF fields (>100 mT) the behavior in the Arai diagram (panel b)
940 sometimes becomes non-linear, these AF fields are also not interpretable (gray
941 area in lower right corner of panel b). Therefore these Arai diagrams can be
942 faithfully interpreted between 7.5 and 100 mT. The average of the absolute
943 slopes of the linear fits through the data from the different samples are the
944 pseudo-Thellier results, as indicated.
945
946 Fig. 5 – Recalibrating the pseudo-Thellier method. For all sites that yielded an
947 acceptable pseudo-Thellier result and acceptable results in one or more other
948 (thermal) paleointensity methods those results are plotted against each other

949 (pseudo-Thellier vs. IGRF or GUFM1 models for flows younger than 1840 AD in
950 yellow triangles, vs. IZZI Thellier in green squares, vs. microwave Thellier in
951 purple diamonds, and vs. MSP-DSC in red circles). The error bars are one
952 standard deviation error envelopes; all data are from de Groot et al. (2013) and
953 this study. The linear fit through all data (blue line) gives an improved
954 calibration relation (B_{abs} = 7.994 × pseudo-Thellier slope + 13.789). The
955 calibration relation from de Groot et al. (2013) (red line) is well within the
956 confidence interval of the new calibration relation (95%, blue shading). Both fits
957 are faded towards the non-zero y-axis intercept.
958
959 Fig. 6 – Full vector geomagnetic field record. The declination (panel a),
960 inclination (panel b) and intensity (panel c) results for the past 6000 years, with
961 the PFM9K.1b (red line), and SHA.DIF.14k (blue line) models, with their one
962 standard deviation confidence envelopes (color shading). The declination and
963 inclination data from this study are depicted as gray diamonds, with the vertical
964 error bar being the α95 interval; data of Kissel et al. (2015) are open circles, Ferk
965 et al. (2011) open diamonds, GEOMAGIA.v3 (Donadini et al., 2006; Korhonen et
966 al., 2008) open squares (GEOMAGIA.v3 query: data type: all; age: -4500 to 2000
967 AD; geographical region: Europe / Canary Islands). In the paleointensity panel
968 (c) IZZI-Thellier results are green squares; microwave Thellier results are purple
969 diamonds; red circles are the MSP-DSC results; blue triangles are the pseudo-
970 Thellier results. Data of Ferk et al. (2011) are open diamonds; GEOMAGIA.v3
971 data are open squares. The vertical error bars indicate one–standard-deviation
972 confidence intervals; in some cases the confidence intervals are very narrow and
973 the error bars are not larger than the data points. The horizontal error bars for
974 the data from this study are one-standard-deviation probability intervals of the
975 INTCAL.13 calibration. If more than one interval was obtained, a horizontal thin
976 gray line connects them and the thickness of the bars is equivalent to their
977 relative probability. Per site only one horizontal error bar is given, if the results
978 per site do not overlap, a vertical thin grey line connects them. The horizontal
979 error bars for literature data are depicted as specified in the study (if available).
980

Fig. 7 – Comparing new data to existing data. A compilation of literature data from a 2000 km-radius around the Canary Islands (panel a) and a comparison to paleointensity data reported for the Levant (panel b), expressed as virtual axial dipole moments (VADMs). VADMs included here are an average of at least three successful Thellier-style paleointensity experiments with a standard deviation < 20% of their mean. Data in panel a from Tenerife are violet stars (Ferk et al., 2011), West-Africa are squares (Mitra et al. (2013) in yellow, and Gómez-Paccard et al. (2012b) in red), Portugal are diamonds (Hartmann et al. (2009) in purple, and Nachasova and Burakov (2009) in green), the Azores are triangles (Di Chiara et al. (2014) in red), and Spain are circles (Catanzariti et al. (2012) in pink, Gómez-Paccard et al. (2006b) in light blue, Gómez-Paccard et al. (2008) in dark blue, Gómez-Paccard et al. (2012a) in green, and Gómez-Paccard et al. (2013) in orange). Data form the Levant (panel b) are from Aitken et al. (1984) in black, Genevey et al. (2003) in yellow, Gallet et al. (2006) in green, Gallet and Le Goff (2006) in red, Ben-Yosef et al. (2008) in dark blue, Ben-Yosef et al. (2009) in orange, Shaar et al. (2011) in light blue, Ertepinar et al. (2012) in brown, and Gallet and Butterlin (2014) in pink). The blue line in panel b is a 10-point moving average of the Levant literature data. A compilation of Balkan data (Tema et al., 2011) is the gray line, with its uncertainty (gray shading). Data from the present study is superimposed on the literature data in both panels (larger symbols: thermal Thellier green squares, microwave Thellier purple diamonds, MSP-DSC red circles, and pseudo-Thellier blue triangles). The averages per cooling unit (Table 3) are connected by a red line. The implications of a possibly incorrect dating of site TF-2 (see main text) are indicated by a gray arrow and red dashed lines.

Table 1 – Site details. For all sites in this study the following is provided: the rock-magnetic group (see χ-T analysis in section 3.1.); location in UTM coordinates (UTM zone 28R); its age (median probability age obtained using the INTCAL.13 calibration of radiocarbon results (pre-1492 AD), or historical age (post-1492)); the one standard deviation probability intervals obtained by the calibration of the radiocarbon datings; the dating sample (TFC- and CITF-

1014 samples from Carracedo et al. (2007) and GCR-samples from Rodriguez-Gonzalez
1015 et al. (2009)) and the laboratory ^{14}C age. The independent cooling units are
1016 identified by the prefix TF or GC (for Tenerife and Gran Canaria, respectively), a
1017 number (^{14}C sites) or year (historical flows); if one cooling unit was sampled at
1018 more than one location these locations are indicated by a character following the
1019 site number.
1020
1021 Table 2 – Geomagnetic directions. For 11 sites in this study paleomagnetic
1022 directions could be obtained. Per site the median probability age, number of
1023 independent samples (n, with the number of samples outside a 45 ° cut-off
1024 between brackets), the mean declination; the mean inclination (inc), the
1025 precision parameter (k), and the 95% cone of confidence (α95) are specified.
1026
1027 Table 3 – Paleointensity results. All successful paleointensity results are grouped
1028 per site (site) and therefore age (median age). For each result the paleointensity
1029 method (IZZI = thermal IZZI-Thellier, MW = microwave Thellier, MSP-DSC =
1030 MSP-DSC method, and pTh = pseudo-Thellier (based on the updated calibration
1031 relation)); the number of samples (pTh and MSP-DSC) or the number of data
1032 points interpreted (IZZI and MW) (N); the paleointensity in μT, the standard
1033 deviation (SD) of the respective interpretation, the corresponding lower and
1034 upper bounds of the confidence interval and the standard error (SE) over the
1035 paleointensity are specified. Per site the results of the different methods are
1036 averaged and the standard error is calculated (the fraction of the standard error
1037 over the average between brackets). The standard deviation of the MSP-DSC
1038 results is asymmetric, therefore lower and upper bounds are given and the
1039 standard error/paleointensity is calculated as follows (upper bound – lower
1040 bound)/(2 x paleointensity) and preceded by a tilde.

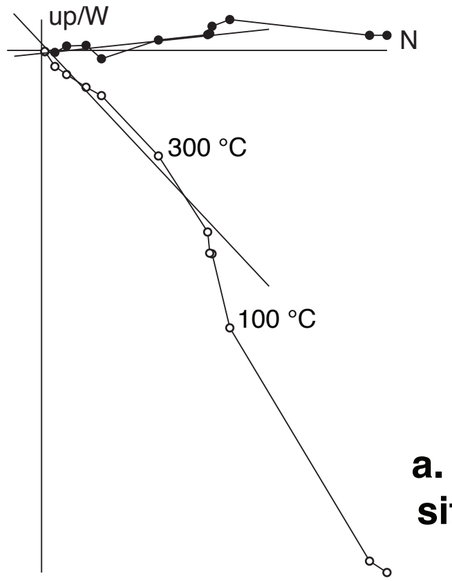

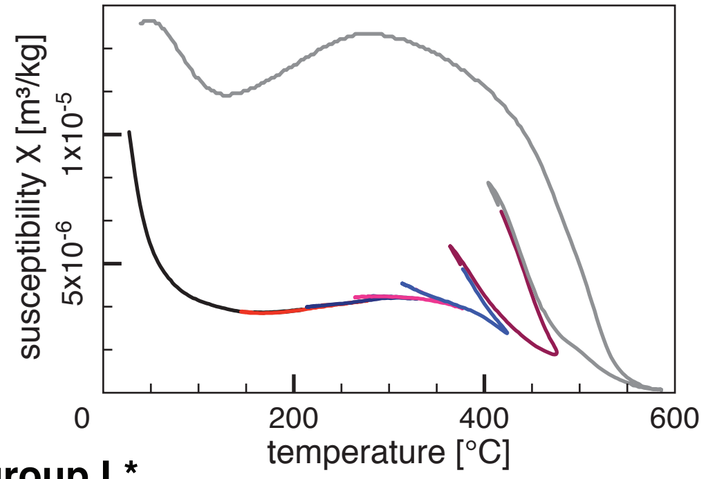

a. group L*
site GC-73

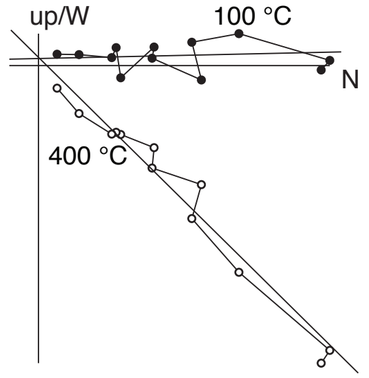

e. group M
site TF-1492

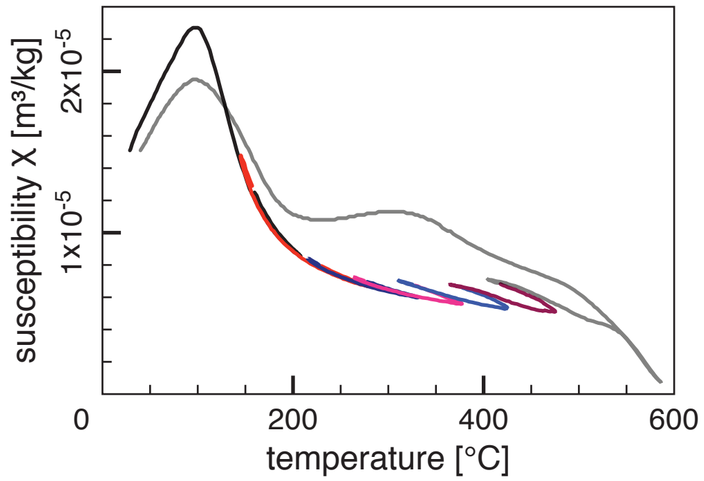

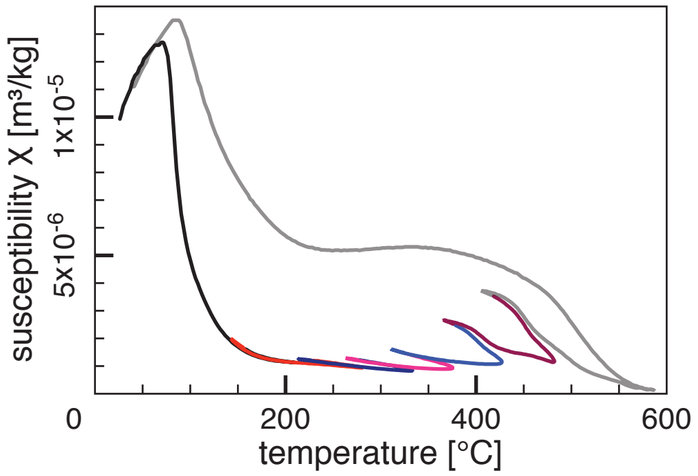

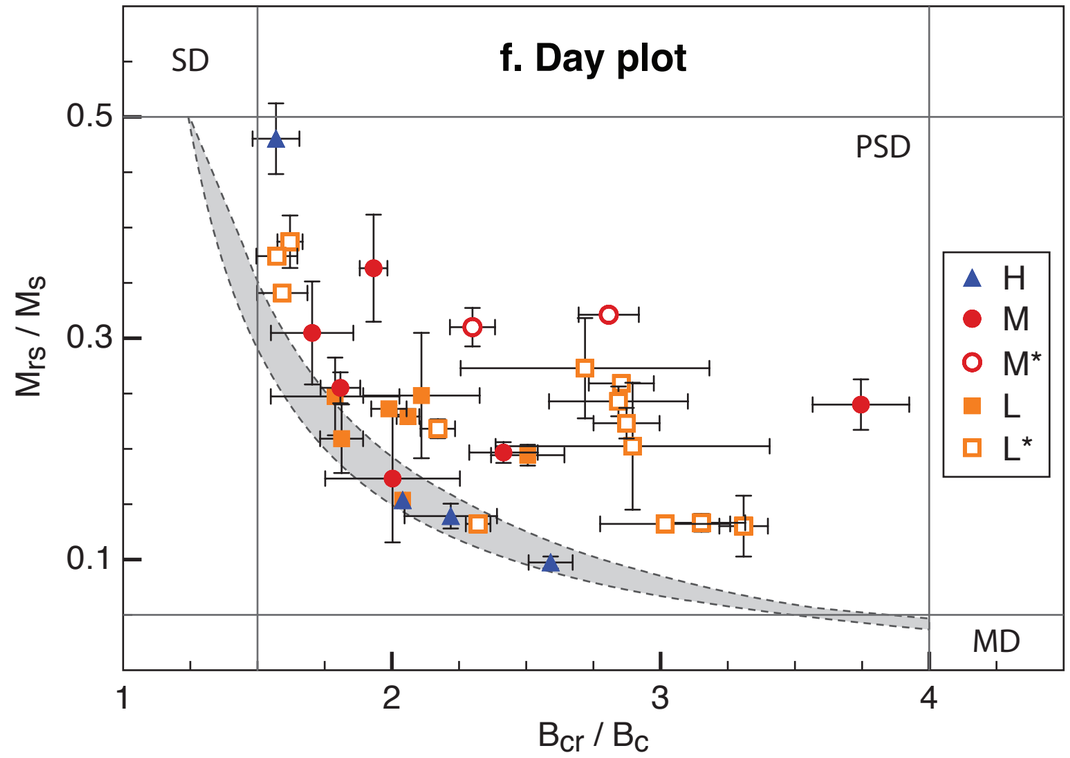

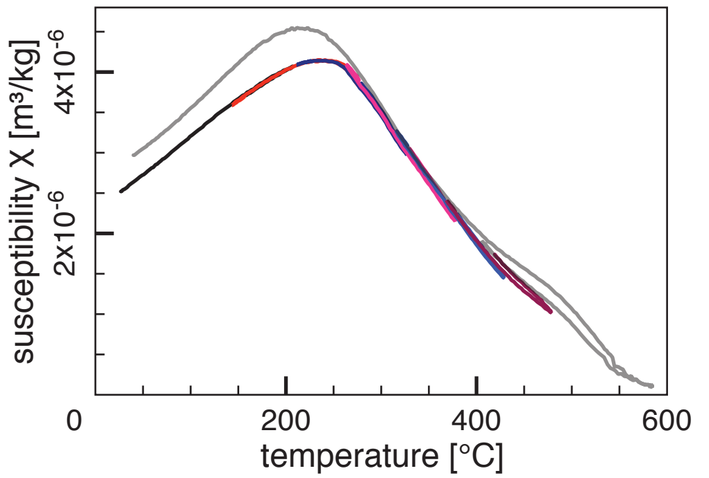

b. group L
site TF-2

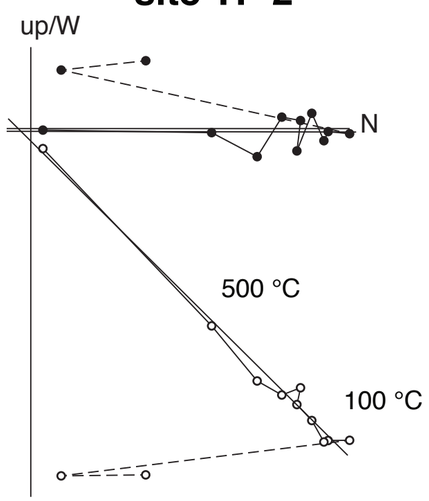

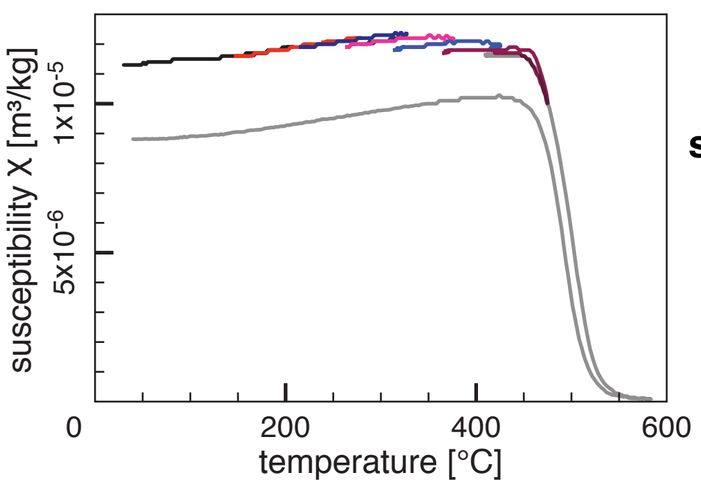

c. group H
site TF-1706

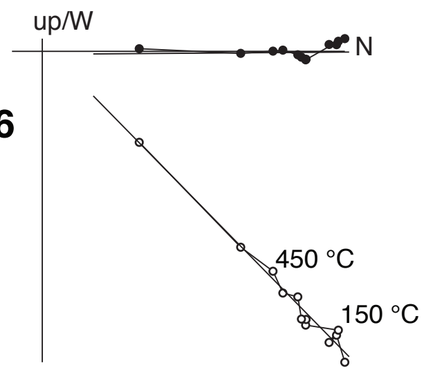

d. group M*
site TF-11

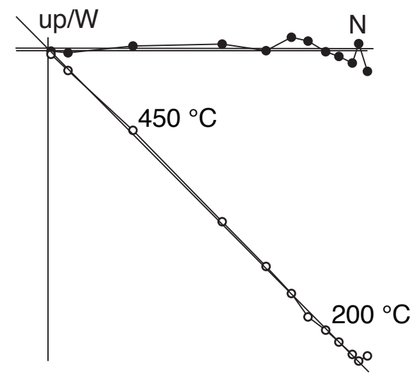

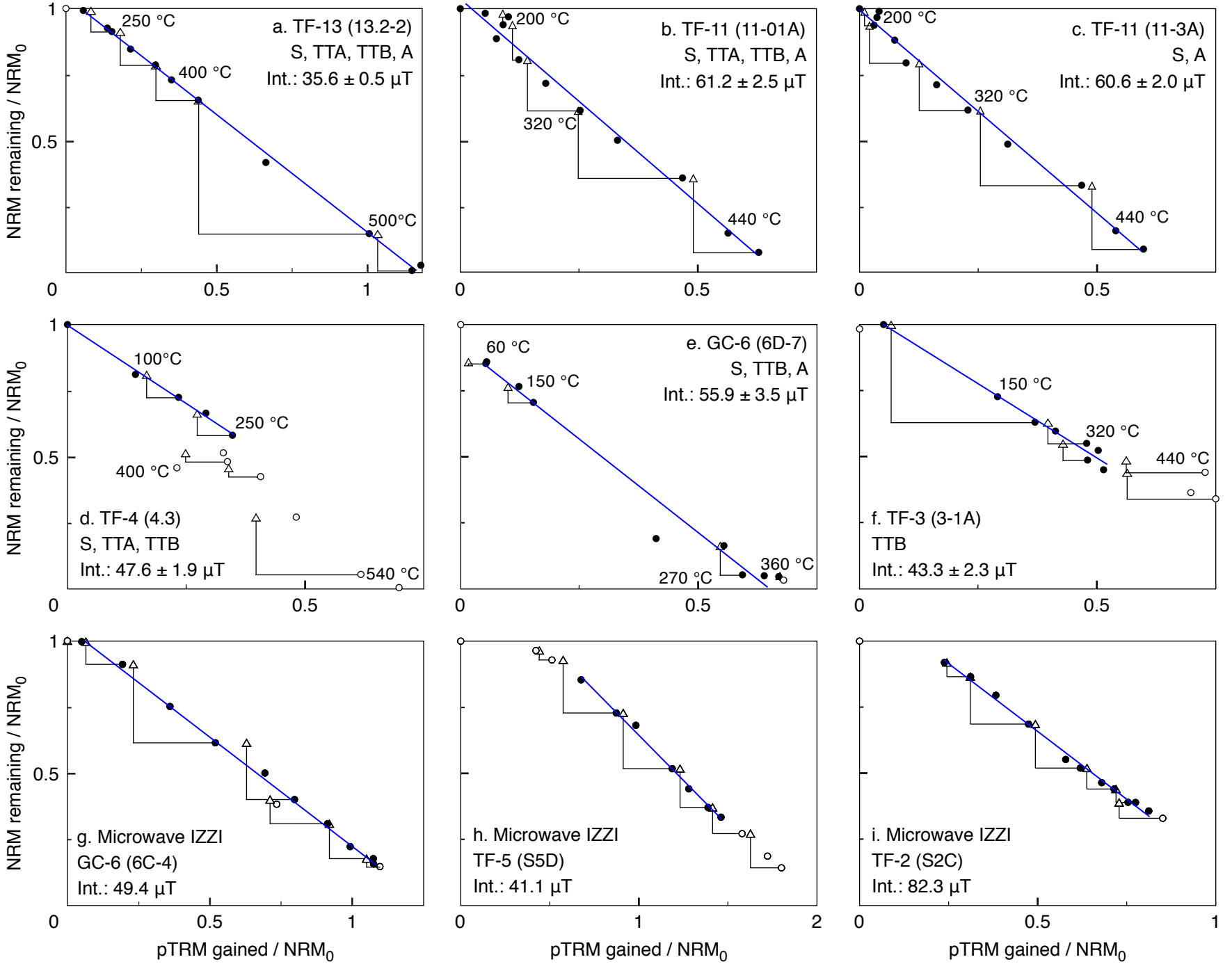
a. TF-13 (13.2-2)
S, TTA, TTB, A
Int.: 35.6 ± 0.5 µT
250 °C
400 °C
500°C
b. TF-11 (11-01A)
S, TTA, TTB, A
Int.: 61.2 ± 2.5 µT
200 °C
320 °C
440 °C
c. TF-11 (11-3A)
S, A
Int.: 60.6 ± 2.0 µT
200 °C
320 °C
440 °C
d. TF-4 (4.3)
S, TTA, TTB
Int.: 47.6 ± 1.9 µT
100°C
250 °C
400 °C
540 °C
e. GC-6 (6D-7)
S, TTB, A
Int.: 55.9 ± 3.5 µT
60 °C
150 °C
270 °C
360 °C
f. TF-3 (3-1A)
TTB
Int.: 43.3 ± 2.3 µT
150 °C
320 °C
440 °C
g. Microwave IZZI
GC-6 (6C-4)
Int.: 49.4 µT
h. Microwave IZZI
TF-5 (S5D)
Int.: 41.1 µT
i. Microwave IZZI
TF-2 (S2C)
Int.: 82.3 µT
NRM remaining / NRM0
pTRM gained / NRM0

a. TF-11, int: 50.6 µT (45.4 - 55.6)

b. GC-73; int: 52.8 µT (51.3 - 54.3)

c. ARM-test TF-11

d. GC-6, int: 47.7 µT (44.0 - 51.5)

e. ARM-test GC-73

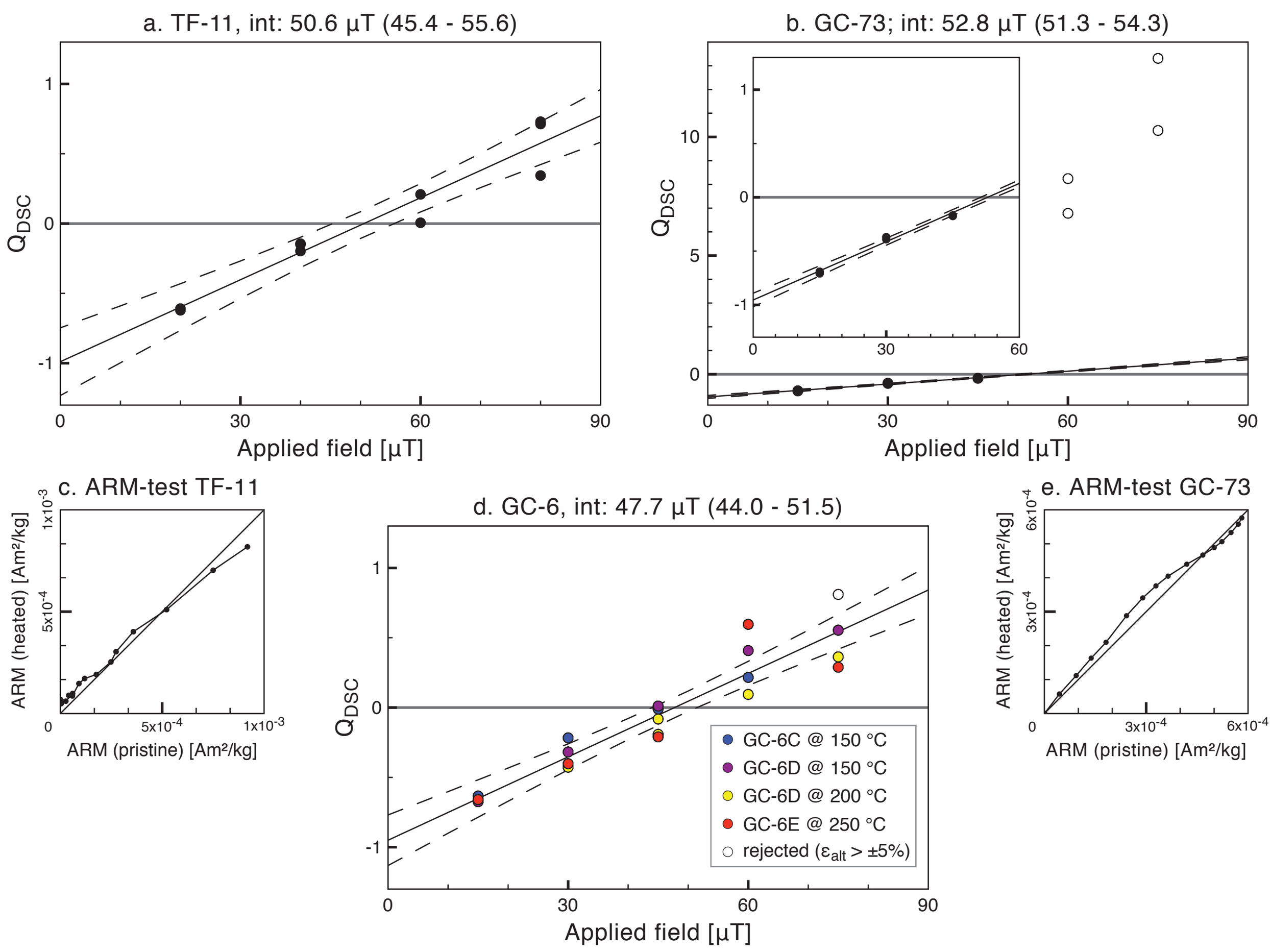

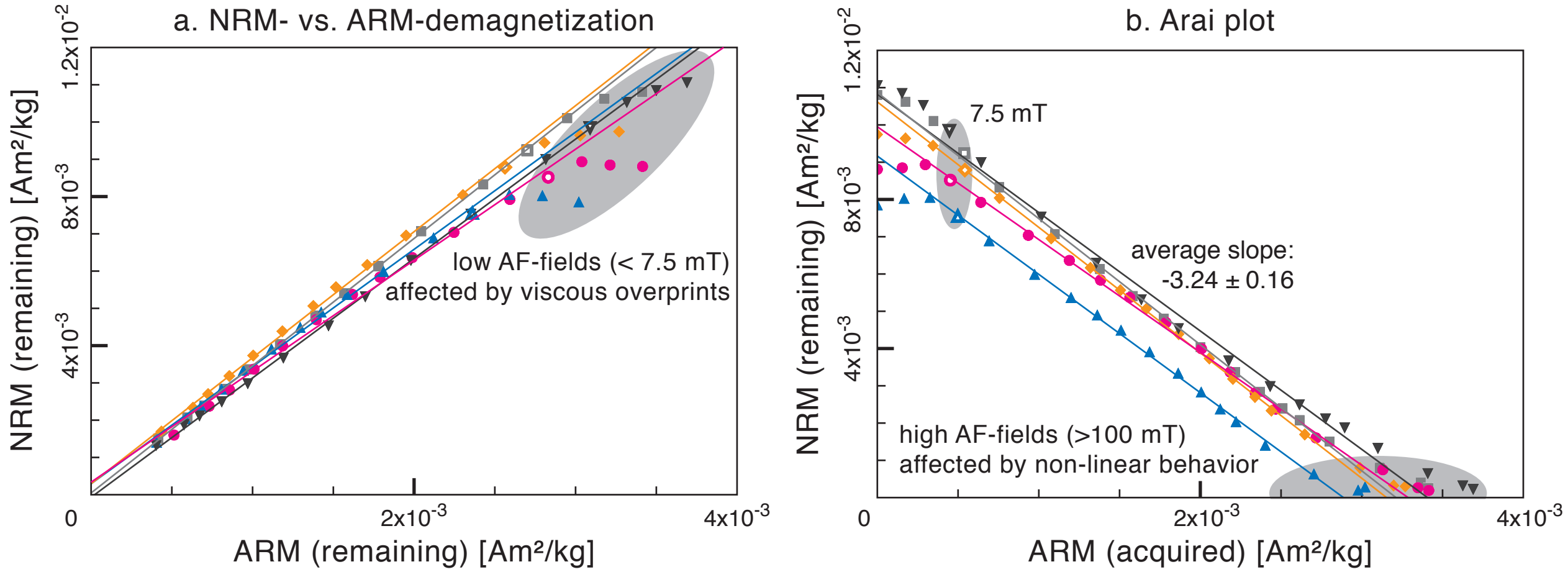
a. NRM- vs. ARM-demagnetization
NRM (remaining) [Am²/kg]
1.2x10-2
8x10-3
4x10-3
0
2x10-3
4x10-3
ARM (remaining) [Am²/kg]
low AF-fields (< 7.5 mT)
affected by viscous overprints
b. Arai plot
NRM (remaining) [Am²/kg]
1.2x10-2
8x10-3
4x10-3
0
2x10-3
4x10-3
ARM (acquired) [Am²/kg]
7.5 mT
average slope:
-3.24 ± 0.16
high AF-fields (>100 mT)
affected by non-linear behavior

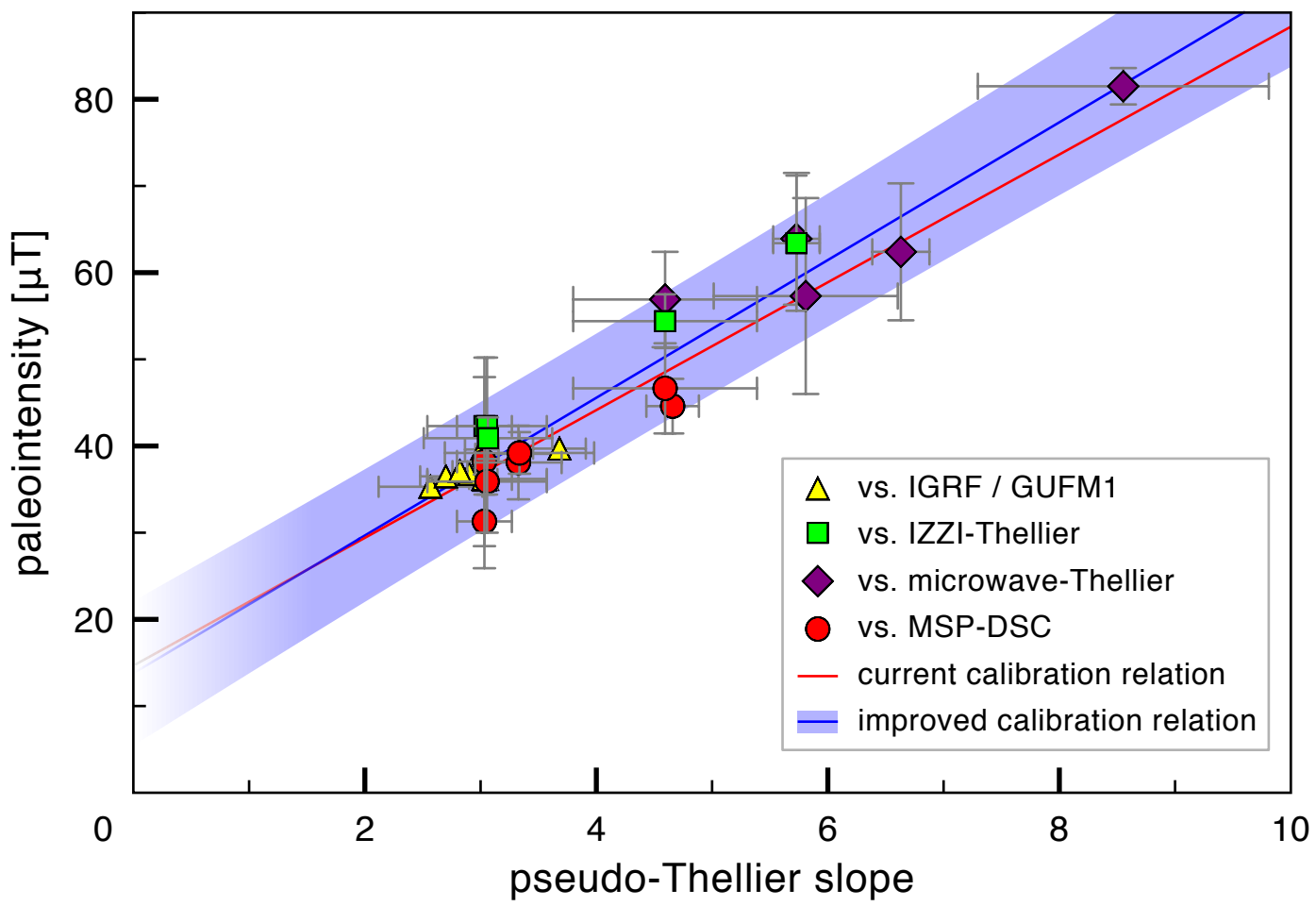
paleointensity [µT]
80
60
40
20
0
2
4
6
8
10
pseudo-Thellier slope
vs. IGRF / GUFM1
vs. IZZI-Thellier
vs. microwave-Thellier
vs. MSP-DSC
current calibration relation
improved calibration relation

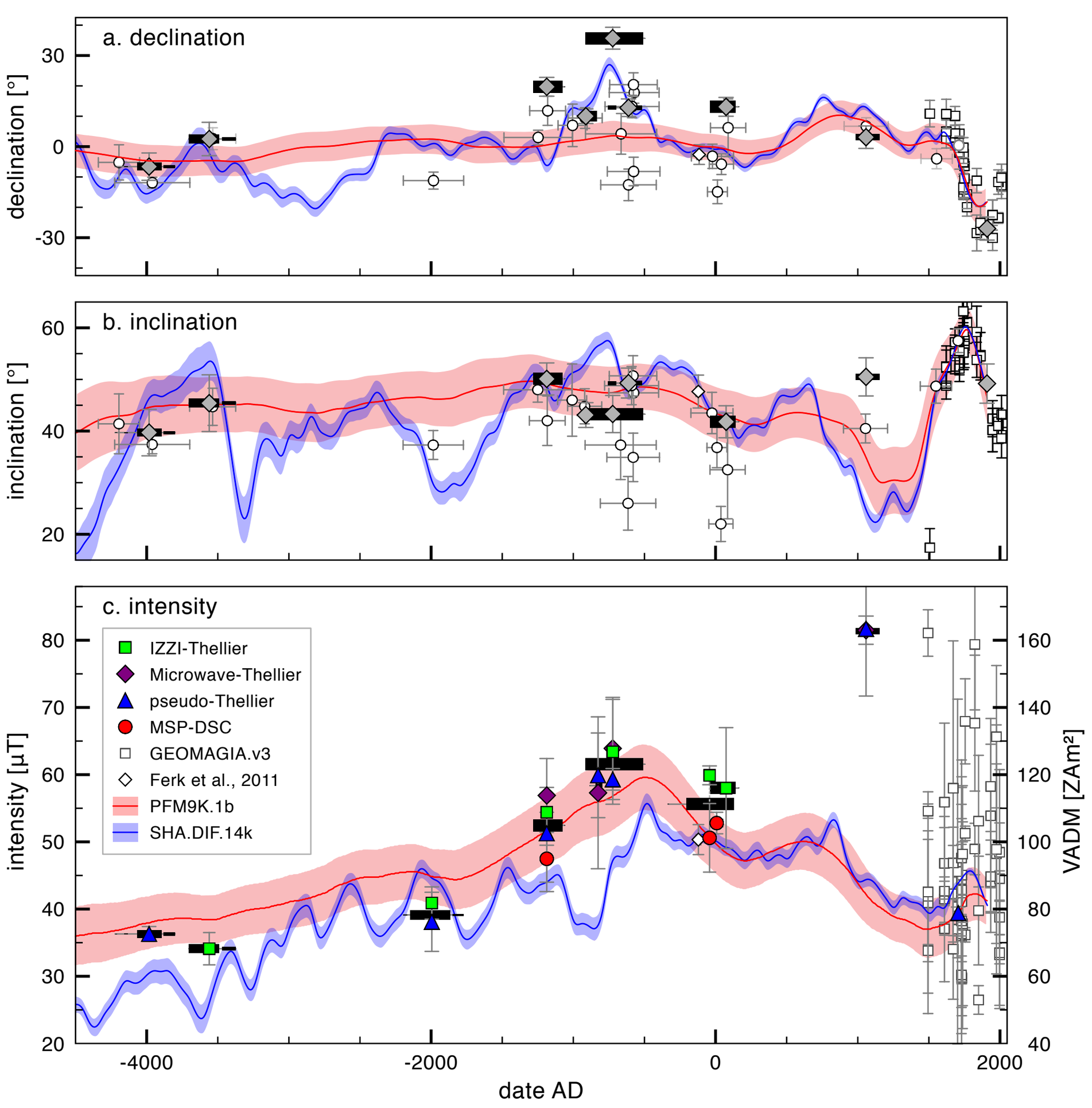
a. declination
declination [°]
30
0
-30
b. inclination
inclination [°]
60
40
20
c. intensity
IZZI-Thellier
Microwave-Thellier
pseudo-Thellier
MSP-DSC
GEOMAGIA.v3
Ferk et al., 2011
PFM9K.1b
SHA.DIF.14k
intensity [µT]
80
70
60
50
40
30
20
VADM [ZAm²]
160
140
120
100
80
60
40
-4000
-2000
0
2000
date AD

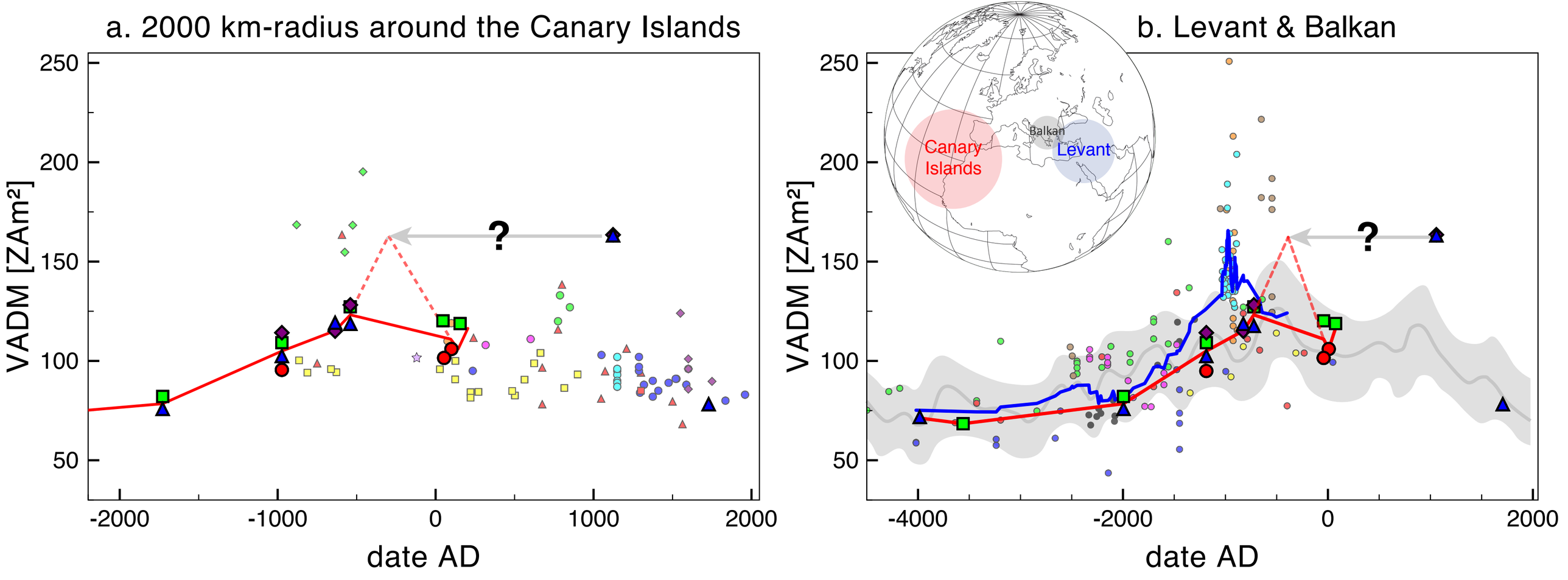
a. 2000 km-radius around the Canary Islands
b. Levant & Balkan
VADM [ZAm²]
date AD
?
Canary Islands
Balkan
Levant
250
200
150
100
50
-2000
-1000
0
1000
2000
-4000

Site	Rock mag.	Location [UTM]		(Calibrated) age	One standard deviation intervals [lower bound – upper bound; relative probability]				Dating sample	^{14}C-age
TF-1909A	L	324752	3131746	1909						
TF-1909B	L*	326848	3130665	1909						
TF-1798A	L*	332754	3125462	1798						
TF-1798B	L*	332754	3125462	1798						
TF-1798C	L*	333741	3124222	1798						
TF-1798D	L*	332754	3125462	1798						
TF-1798E	L*	333741	3124222	1798						
TF-1706	H	326786	3135197	1706						
TF-1492	M	326634	3129562	1492						
TF-2	L	327595	3132121	1058 AD	987 – 1056 AD; 0.488	1076 – 1154 AD; 0.512			TFC-369	990 ± 70
TF-9A	H	332814	3135598	235 AD	89 - 100 AD; 0.033	123 - 382 AD; 0.967			TFC-25	1790 ± 120
TF-9B	H	332795	3135625	235 AD	89 - 100 AD; 0.033	123 - 382 AD; 0.967			TFC-25	1790 ± 120
TF-3	M	331425	3125118	74 AD	40 BC - 140 AD; 0.941	160 - 165 AD; 0.020	196 - 208 AD; 0.038		TFC-219	1930 ± 80
GC-73	L*	448157	3092155	8 AD	38 - 8 BC; 0.323	4 BC - 53 AD; 0.677			GCR-73	1990 ± 40
TF-11	M*	339309	3133172	42 BC	337 - 329 BC; 0.017	204 BC - 130 AD; 0.983			TFC-02	2020 ± 140
GC-60	L*	457291	3100098	612 BC	756 - 679 BC; 0.350	671 - 605 BC; 0.291	598 - 516 BC; 0.359		GCR-60	2470 ± 50
TF-4	M	324650	3133033	723 BC	914 - 509 BC; 0.996	497 - 495 BC; 0.004			TFC-138	2600 ± 160
TF-5	L	325906	3133153	826 BC	887 - 884 BC; 0.019	843 - 797 BC; 0.981			TFC-375	2660 ± 40
GC-64A	L*	434565	3105941	912 BC	974 - 954 BC; 0.136	943 - 834 BC; 0.864			GCR-64	2760 ± 60
GC-64B	L*	434565	3105941	912 BC	974 - 954 BC; 0.136	943 - 834 BC; 0.864			GCR-64	2760 ± 60
GC-64C	L*	434565	3105941	912 BC	974 - 954 BC; 0.136	943 - 834 BC; 0.864			GCR-64	2760 ± 60
GC-45	L*	439107	3102273	994 BC	1074 - 1065 BC; 0.032	1057 - 906 BC; 0.968			GCR-45	2830 ± 60
GC-6C	L	439834	3100061	1187 BC	1282 - 1076 BC; 0.976	1064 -1058 BC; 0.024			GCR-6	2970 ± 70
GC-6D	L	439834	3100061	1187 BC	1282 - 1076 BC; 0.976	1064 -1058 BC; 0.024			GCR-6	2970 ± 70
GC-6E	L	439834	3100061	1187 BC	1282 - 1076 BC; 0.976	1064 -1058 BC; 0.024			GCR-6	2970 ± 70
GC-47A	L	434892	3104525	1266 BC	1406 - 1191 BC; 0.912	1176 - 1163 BC; 0.043	1144 - 1131 BC; 0.046		GCR-47	3030 ± 90
GC-47B	L*	434892	3104525	1266 BC	1406 - 1191 BC; 0.912	1176 - 1163 BC; 0.043	1144 - 1131 BC; 0.046		GCR-47	3030 ± 90
TF-6A	M	332519	3125886	1995 BC	2196 - 2169 BC; 0.057	2148 - 1865 BC; 0.780	1849 - 1773 BC; 0.163		TFC-56	3620 ± 140
TF-6B	M	332584	3125930	1995 BC	2196 - 2169 BC; 0.057	2148 - 1865 BC; 0.780	1849 - 1773 BC; 0.163		TFC-56	3620 ± 140
TF-13A	M	339977	3133533	3560 BC	3704 - 3492 BC; 0.719	3470 - 3373 BC; 0.281			TFC-01	4790 ± 140
TF-13B	M*	339977	3133533	3560 BC	3704 - 3492 BC; 0.719	3470 - 3373 BC; 0.281			TFC-01	4790 ± 140
TF-14	H	340578	3133782	3983 BC	4222 - 4209 BC; 0.036	4157 - 4132 BC; 0.066	4067 - 3895 BC; 0.634	3881 - 3800 BC; 0.265	CITF-60	5170 ± 110

site	median age	n (rejected)	declination [°]	inclination [°]	k	α95
TF-1909A	1909 AD	9	-27.0	49.2	184.5	3.8
TF-2	1058 AD	7	3.1	50.5	264.4	3.7
TF-3	74 AD	8	13.1	41.8	319.4	3.1
GC-73	8 AD	8	-20.0	39.4	52.9	7.7
GC-60	612 BC	12	12.8	49.3	232.8	2.9
TF-4	723 BC	9	35.7	43.3	207.2	3.6
GC-64	912 BC	34	10.0	43.1	105.2	2.4
GC-6	1187 BC	9	19.7	50.1	281.6	3.1
GC-47	1266 BC	14 (1)	13.1	42.9	5.6	19.2
TF-13A	3560 BC	5	2.5	45.4	191.5	5.5
TF-14	3983 BC	7	-6.6	39.7	177	4.5

Site	Median age	Method	N	Paleoint. [μT]	SE [μT]	Lower bound [μT]	Upper bound [μT]	SE /paleoint.
TF-1706	1706 AD	pTh	4	39.4	0.9	38.5	40.3	2.3%
TF-2	1058 AD	MW	3	81.5	2.1	79.4	83.6	2.6%
TF-2	1058 AD	pTh	6	81.7	10.0	71.7	31.7	12.2%
		Average		**81.6**				
		SE		0.1 (0.1%)				
TF-3	74 AD	IZZI	4	58.0	9.0	49.0	67.0	15.5%
GC-73	8 AD	MSP-DSC	10	52.8	-	51.3	54.5	~3.0%
TF-11	42 BC	IZZI	3	59.9	1.4	58.5	61.4	2.4%
TF-11	42 BC	MSP-DSC	5	50.6	-	45.4	55.6	~10.1%
		Average		**55.3**				
		SE		4.7 (8.4%)				
TF-4	723 BC	IZZI	6	63.4	7.8	55.5	71.2	12.4%
TF-4	723 BC	MW	3	63.9	7.6	56.3	71.5	11.9%
TF-4	723 BC	pTh	4	59.3	1.6	57.7	60.9	2.7%
		Average		**62.2**				
		SE		2.1 (3.3%)				
TF-5	826 BC	MW	4	57.3	11.3	46.0	68.6	19.8%
TF-5	826 BC	pTh	6	59.9	6.3	53.6	66.3	10.5%
		Average		**58.6**				
		SE		1.3 (2.2%)				
GC-6	1187 BC	**IZZI**	**7**	**54.4**	**3.1**	**51.3**	**57.5**	**5.7%**
GC-6	1187 BC	MW	3	56.9	5.5	51.4	62.4	9.7%
GC-6	1187 BC	MSP-DSC	19	47.7	-	44.0	51.5	~7.9%
GC-6	1187 BC	pTh	4	50.3	6.3	43.0	48.1	5.6%
		Average		**52.3**				
		SE		3.6 (6.8%)				
TF-6	1995 BC	IZZI	3	40.9	2.4	38.5	43.3	5.9%
TF-6	1995 BC	pTh	10	38.1	4.4	33.7	42.5	11.6%
		Average		**39.5**				
		SE		1.4 (3.5%)				
TF-13	3560 BC	IZZI	5	34.1	2.4	31.7	36.5	7.0%
TF-14	3983 BC	pTh	4	36.3	1.1	35.2	37.3	3.0%